

Quantum criticality of fermion velocities and critical temperature nearby a putative quantum phase transition in the d -wave superconductors

Xiao-Yue Ren, Ya-Hui Zhai, and Jing Wang*

Department of Physics, Tianjin University, Tianjin 300072, P.R. China

(Dated: September 24, 2021)

Quantum critical behaviors induced by a putative quantum phase transition are vigilantly investigated, which separates a d -wave superconducting and d -wave superconducting+ X state below the superconducting dome of the d -wave superconductors with tuning the non-thermal doping variable. Within the framework of renormalization group approach, we start with a phenomenological effective theory originated from the Landau-Ginzburg-Wilson theory and practice one-loop calculations to construct a set of coupled flows of all interaction parameters. After extracting related physical information from these coupled evolutions, we address that both fermion velocities and critical temperatures exhibit critical behaviors, which are robust enough against the initial conditions due to strong quantum fluctuations. At first, the evolution of Yukawa coupling between X -state order parameter and nodal fermions in tandem with quantum fluctuations heavily renormalize fermion velocities and generally drive them into certain finite anisotropic fixed point at the lowest-energy limit, whose concrete value relies upon the very quantum phase transition. In addition, these unique properties of fermion velocities largely reshape the fate of superfluid density, giving rise to either an enhancement or a dip of critical temperature. Moreover, we find that fermion-fermion interactions bring non-ignorable quantitative corrections to quantum critical behaviors despite they are subordinate to quantum fluctuations of order parameters.

PACS numbers: 74.72.-h, 73.43.Nq, 74.20.De, 74.25.Dw

I. INTRODUCTION

A plethora of both theoretical and experimental research efforts have been devoted to the d -wave cuprate superconductors in the last three decades owing to their unique pairing mechanisms and anomalous properties in the normal states [1–27]. Compared to their s -wave counterparts [5, 6, 27], it is noteworthy that such superconductors own a $d_{x^2-y^2}$ superconducting gap [2, 16, 28–32], which vanishes at four nodes $(\pm\pi/2, \pm\pi/2)$ in the first Brillouin zone [2, 16, 25]. This indicates that the gapless nodal quasiparticles (QPs) can be excited from these nodal points and present even at the lowest energy in the superconducting phase [8, 10, 14, 16, 31]. Generally, these nodal QPs are nearly non-interacting and have a rather long lifetime [31]. However, this feature can be significantly changed once the nodal fermions interact with certain critical bosonic mode accompanied by a quantum phase transition (QPT) [33–35], around which the quantum fluctuations couple strongly to the nodal fermions, giving rise to severe fermion damping [11–13, 19, 36] and other striking properties [17, 20, 22, 37–39]. It is therefore reasonably expected that these nodal QPs together with quantum critical degrees of freedom would be responsible for unusual behaviors around the QPT [16, 23–25, 31–44].

On the basis of diversities and complexities of realistic systems, a series of stimulated frameworks are proposed [8–12, 34, 45–47] to explore and unravel the in-

timite connection between quantum criticality and unusual properties associated with nodal QPs in the d -wave superconductors. One of the most well-known pioneering scenarios was put forward by Vojta *et al.* in 2000 [11–13]. Within their strategy, a putative quantum critical point (QCP) [33, 35] exists somewhere in the superconducting dome accompanied by certain QPT from a $d_{x^2-y^2}$ superconducting state to another $d_{x^2-y^2} + X$ superconducting state as schematically presented in Fig. 1 due to the topological changes of nodal positions [11–13]. Hereby, the X state is developed by the C_4 symmetry breaking of nodal positions and owns seven potential candidates based upon the group-theory analysis [11–13]. These states can be effectively reduced to four distinct types [48], which are associated with the QPTs denominated by Type- $\tau_{0,x,y,z}$ in this work. In the proximity of a QCP, the quantum fluctuation of X order parameter strongly couples to gapless nodal QPs, which then leads to nontrivial critical effects on two fermion velocities of nodal QPs consisting of the Fermi velocity v_F and the gap velocity v_Δ [45, 49]. In particular, their ratio v_Δ/v_F plays an important role in pinning down the low-energy fates of physical quantities in that it always enters into a number of important observable quantities including the superfluid density and critical temperature [50] as well as electric and thermal conductivities [45, 49, 51, 52]. This signals any unusual renormalization of this velocity ratio will give rise to certain enhancement or suppression of these observable quantities. It is therefore of considerable necessity to explore the low-energy tendency of v_Δ/v_F . Stimulated by this, Huh and Sachdev [17] carefully examine the Type- τ_x QPT, which is so-called nematic QPT with spontaneously breaking C_4 symmetry down to C_2

*Corresponding author: jing.wang@tju.edu.cn

symmetry of the system [7, 11, 12, 17–20, 35, 37, 52–62], and obtain a fixed point $v_\Delta/v_F \rightarrow 0$ at the lowest-energy limit. In addition, Wang *et al.* [48, 63, 64] address two distinct fixed points corresponding to $v_\Delta/v_F \rightarrow 1$ and $v_\Delta/v_F \rightarrow \infty$ for Type- τ_y and Type- τ_z QPTs, respectively. Further, the consequences of these fixed points on the physical implications are subsequently investigated in Refs. [18–20, 22, 48, 63, 64].

Despite of these considerable progresses on the behaviors of fermion velocities nearby the QPTs [17–20, 22, 38, 48, 63, 64], several quantum critical degrees of freedom are insufficiently taken into account, which may be essential to dictate the low-energy behaviors of the system. On one hand, the Yukawa coupling between nodal QPs and certain order parameter is fixed as an energy-independent constant to approximately collect the physical ingredients nearby the QPTs in these works [17–20, 22, 38, 48, 63, 64]. Going beyond this fixed-coupling assumption, much more physical information would be captured and hence the low-energy fates of fermion velocities may be partially or heavily modified by the coupled entanglements of all interaction parameters due to quantum criticality. On the other hand, although the nodal fermions are always excited [16], they own a long lifetime and can coexist with the superconducting state [31]. This implies the fermion-fermion interactions can be safely neglected away from the QCP. However, quantum criticality would coax these nodal QPs to mutually intertwine with each other and influence fermion velocities plus Yukawa coupling. Consequently, fermion-fermion interactions may play important roles in determining critical behaviors around certain QCP [65–79, 81–98, 104]. Consequently, one can expect that uncovering the contributions from these two quantum critical ingredients may well improve our understandings on the quantum criticality of certain QCP in the d -wave superconductor.

In order to encapsulate more physical information driven by the QCP, it is therefore imperative to systematically investigate the effects of fermion-order parameter couplings and fermion-fermion interactions as well as their interplay on the low-energy fates of fermion velocities and related observable quantities. To this purpose, we within this work employ the momentum-shell renormalization group (RG) approach [99–101] to unbiasedly treat all these critical physical degrees of freedom nearby a putative QPT from the d -wave superconducting to d -wave superconducting+ X state as illustrated in Fig. 1. After collecting all one-loop corrections, a set of coupled RG flows of all interaction parameters are derived to characterize the quantum criticality nearby all four types of potential QPTs dubbed Type- $\tau_{0,x,y,z}$ that are explicitly clarified in Sec. II A.

Decoding the physical information contained in the coupled RG equations yields a number of quantum critical properties in the vicinity of all QCPs. At first, we find that the fermion velocities exhibit several interesting fixed points. With respect to the Type- τ_0 QPT, the

Yukawa interplay designated as λ between nodal QPs and related order parameter is marginal to one-loop level and the ratio of fermion velocities flows towards either fixed point $(v_\Delta/v_F)^* \approx 0.3478$ or $(v_\Delta/v_F)^* \approx 0.0942$ at the low-energy limit caused by the quantum criticality. Concerning Type- $\tau_{x,y,z}$ QPTs, the evolution of Yukawa coupling λ and quantum fluctuations heavily reshape three fixed points $v_\Delta/v_F \rightarrow 0, 1, \infty$ for Type- $\tau_{x,y,z}$ under the fixed-coupling assumptions [17, 48] to evolve towards finite anisotropies as approaching the QPTs. To be specific, the extreme anisotropies of fermion velocities are changed to finite anisotropies for both Type- $\tau_{x,z}$ QPTs but instead the isotropic fermion velocities for Type- τ_y QPT are broken and attracted by a finite anisotropic fixed point. In addition, we notice that the unusual behaviors of fermion velocities considerably modify the fates of superfluid density and critical temperature around the underlying four types of QPTs. As approaching the Type- $\tau_{0,x}$ QPTs, the critical temperature is largely suppressed. Conversely, both Type- τ_y and Type- τ_z QPTs are in favor of the superconductivity. Furthermore, the roles of fermion-fermion interactions that have not yet been adequately considered are also inspected in quantum criticality. We realize that they can give rise to quantitative contributions to quantum critical behaviors in the vicinity of all putative QPTs. Last but not the least important, it is worth pointing out that our qualitative results are considerably robust enough with the variation of initial conditions.

The rest of paper is organized as follows. In Sec. II, we establish our low-energy effective field theory that includes the most of key physical ingredients to describe the main physics around the QPT. On the basis of the effective theory, we within Sec. III perform one-loop momentum-shell RG analysis to deliver the coupled RG equations of all interaction parameters. After combining both the tentatively analytical discussions and vigilant numerical calculations, Sec. IV and Sec. V are followed to present the critical behaviors of fermion velocities and superfluid density together with critical temperature nearby the QCP, respectively. Finally, we provide a brief summary in Sec. VI.

II. EFFECTIVE THEORY

In this work, our focus is put on a putative QPT in the d -wave superconductor as schematically displayed in Fig. 1 as well as the associated critical behaviors of fermion velocities and physical quantities. To begin with, we within this section are going to construct the low-energy effective field theory around the QPT and defer the one-loop RG analysis to the next section III.

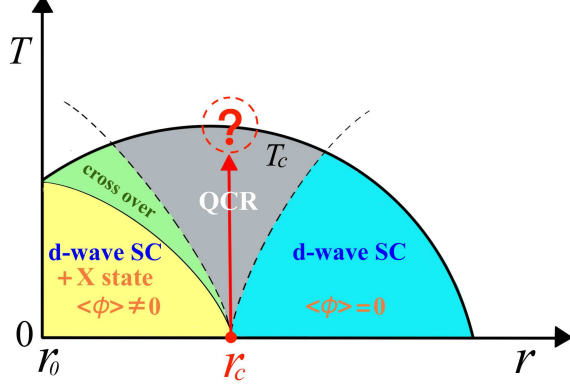


FIG. 1: (Color online) Schematic illustration for some potential quantum phase transition (QPT) from a d -wave SC to d -wave SC+ X state beneath the superconducting dome of the d -wave superconductor with tuning the non-thermal doping variable [11]. Hereby, T_c denotes the critical temperature of d -wave superconductor and the field ϕ characterizes the order parameter of X state, which depends upon the specific symmetry breaking accompanied by the QPT. In addition, the very value r_c that roughly locates at the optimal doping is the so-called quantum critical point (QCP), which separates the disordered ($\langle\phi\rangle = 0$) and ordered ($\langle\phi\rangle \neq 0$) X phases at $T = 0$. As to the finite-temperature region around the QPT, critical behaviors are expected to be induced in the quantum critical region (QCR) due to the strong quantum fluctuations. The fate of critical temperature circled by the dashed line will be explicitly addressed in Sec. V.

A. Phenomenological model

As the d -wave superconductor is pushed closer to the QCP depicted in Fig. 1, the possible quantum criticality in the quantum critical region (QCR) can be principally ascribed to three major distinct types of physical ingredients that are gapless fermionic quasiparticles (QP) excited from the nodal points and quantum fluctuation for order parameter ϕ of X state in tandem with their intimate interplay [11–13, 17, 48]. Without loss of generality, the phenomenological model is therefore introduced to capture the physical information nearby the QCP [17, 18, 48],

$$S = S_\Psi + S_{\phi_0} + S_{\Psi\phi_0}, \quad (1)$$

where S_Ψ , S_{ϕ_0} , and $S_{\Psi\phi_0}$ serve as the degrees of fermionic QPs, order parameter, and their couplings, respectively. To be concrete, the gapless fermions with linear dispersion are allowed to be freely excited from four nodes on the Fermi surface and this fermionic part can be expressed as follows [17, 18, 48],

$$S_\Psi = \int \frac{d^2\mathbf{k}}{(2\pi)^2} \frac{d\omega}{2\pi} \Psi_{1a}^\dagger (-i\omega + v_F k_x \tau^z + v_\Delta k_y \tau^x) \Psi_{1a} \\ + \int \frac{d^2\mathbf{k}}{(2\pi)^2} \frac{d\omega}{2\pi} \Psi_{2a}^\dagger (-i\omega + v_F k_y \tau^z + v_\Delta k_x \tau^x) \Psi_{2a}, \quad (2)$$

with $\tau^{x,y,z}$ denoting the Pauli matrices [17, 18, 48]. Hereby, the spinors Ψ_{1a} and Ψ_{2a} with the repeated spin index a being summed from 1 to the number of fermion flavor N are employed to specify the fermionic QPs stemming from nodal points at $(\frac{\pi}{2}, \frac{\pi}{2})$ plus $(-\frac{\pi}{2}, -\frac{\pi}{2})$ and $(-\frac{\pi}{2}, \frac{\pi}{2})$ plus $(\frac{\pi}{2}, -\frac{\pi}{2})$, respectively [11–13, 17]. Besides, as displayed in Fig. 2, the $k_{x,y}$ describe the momenta with relative to the nodal points and $v_{F,\Delta}$ correspondingly serve as the Fermi velocity and gap velocity.

With respect to the order-parameter part, there in all exist seven different sorts of order parameters for the state X in Fig. 1, which are solely determined by the specific symmetry breaking of nodal positions [11–13]. It is of particular significance to point out that the couplings between gapless QPs and order parameters are heavily dependent on the symmetry breaking [11]. As a result, it is convenient to bring about the Yukawa couplings before presenting the S_{ϕ_0} , which are written as [11–13, 17, 18, 48]

$$S_{\Psi\phi_0} = \int d^2\mathbf{x} d\tau [\lambda_0 \phi_0 (\Psi_1^\dagger \mathcal{M}_1 \Psi_1 + \Psi_2^\dagger \mathcal{M}_2 \Psi_2)], \quad (3)$$

where the matrices $\mathcal{M}_{1,2}$ are directly associated with the distinct types of order parameters with λ_0 designating the coupling strength, which are explicitly classified as follows [11–13]: Case-I with $\mathcal{M}_1 = \tau_y, \mathcal{M}_2 = \tau_y$, Case-II with $\mathcal{M}_1 = \tau_y, \mathcal{M}_2 = -\tau_y$, Case-III with $\lambda_0 = 0$ (such situation is trivial and not discussed further), Case-IV with $\mathcal{M}_1 = \tau_x, \mathcal{M}_2 = \tau_x$, Case-V with $\mathcal{M}_1 = \tau_z, \mathcal{M}_2 = -\tau_z$, and Case-VI with $\mathcal{M}_1 = \tau_x, \mathcal{M}_2 = -\tau_x$. In distinction to such six sorts, two real components ϕ_{0A} and ϕ_{0B} constitute the order parameter of Case-VII, which respectively interact with Ψ_1 and Ψ_2 , yielding to [13]

$$S_{\Psi\phi_0} = \int d^2\mathbf{x} d\tau [\lambda_0 (\phi_{0A} \Psi_1^\dagger \mathcal{M}_1 \Psi_1 + \phi_{0B} \Psi_2^\dagger \mathcal{M}_2 \Psi_2)], \quad (4)$$

with $\mathcal{M}_1 = \mathcal{M}_2 = \tau_0$.

To proceed, one can figure out that the matrices \mathcal{M}_1 and \mathcal{M}_2 always appear in pairs during the calculations of one-loop corrections and henceforth the results are insensitive to their signs [11–13, 48]. As a corollary, these seven types of Yukawa couplings can be reduced to another four simplified categories of phase transitions, which are accordingly designated as Type- τ_x with $\mathcal{M}_{1,2} = \tau_x$, Type- τ_y with $\mathcal{M}_{1,2} = \tau_y$, Type- τ_z with $\mathcal{M}_{1,2} = \tau_z$, and Type- τ_0 with $\mathcal{M}_{1,2} = \tau_0$, respectively. In order to be consistent with such version of classification, the corresponding order-parameter part S_{ϕ_0} can be cast as [11–13, 17, 48, 63]

$$S_{\phi_0} = \frac{1}{2} \int \frac{d^3q}{(2\pi)^3} [-2(r - r_c) + q^2] \phi_0^2, \quad (5)$$

for Type- τ_x , Type- τ_y , and Type- τ_z . In comparison, one needs to replace the ϕ_0^2 in Eq. (5) with $(\phi_{0A}^2 + \phi_{0B}^2)$ to obtain their Type- τ_0 counterpart. For convenience, we hereby neglect the order-parameter self-interaction terms

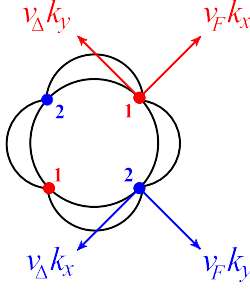


FIG. 2: (Color online) Illustrations for the momenta ($k_{x,y}$) and fermion velocities ($v_{F,\Delta}$) of two pairs of nodal QPs excited from four nodal points of the d -wave superconductor.

(ϕ_0^4) in that they are irrelevant with the support of the power counting [17]. It is worth highlighting that the term $(r - r_c)$ is equivalent to the mass parameter, which is tuned to be zero as the QCP is accessed at $r = r_c$ displayed in Fig. 1.

B. Renormalized order-parameter action and effective theory

Before proceeding further, it is of particular importance to point out that the free order-parameter action (5) would be qualitatively renormalized by one-loop corrections due to switching on the Yukawa couplings between nodal QPs and order parameter. In order to evaluate such effects, we are forced to compute the polarization function of order parameter depicted in Fig. 3(a), which can be formally expressed as [11–13, 17, 48, 63]

$$\Pi(\mathbf{q}, \epsilon) = \int \frac{d^2\mathbf{k}}{(2\pi)^2} \frac{d\omega}{2\pi} \text{Tr}[\mathcal{M}G_\Psi^0(\mathbf{k}, \omega)\mathcal{M}G_\Psi^0(\mathbf{k}+\mathbf{q}, \omega+\epsilon)], \quad (6)$$

with the vertex matrix \mathcal{M} being designated in Eq. (4).

Hereby, the free fermionic propagator can be forwardly derived from Eq. (2) [11, 17]. Specifically, it reads

$$G_\Psi^0(\mathbf{k}, \omega) = \frac{1}{-i\omega + v_F k_x \tau^z + v_\Delta k_y \tau^x}, \quad (7)$$

for nodal QPs Ψ_1 and its Ψ_2 counterpart would be analogously obtained via exchanging the positions of momenta k_x and k_y in Eq. (7).

After performing long but straightforward calculations [17, 18, 48], we are left with one-loop polarization functions for four different types of phase transitions as follows, namely

$$\Pi^{\tau_x}(\mathbf{q}, \epsilon) = \frac{1}{16v_F v_\Delta} \frac{\epsilon^2 + v_F^2 q_x^2}{\sqrt{\epsilon^2 + v_F^2 q_x^2 + v_\Delta^2 q_y^2}} + (q_x \rightarrow q_y), \quad (8)$$

$$\Pi^{\tau_y}(\mathbf{q}, \epsilon) = \frac{1}{16v_F v_\Delta} \sqrt{\epsilon^2 + v_F^2 q_x^2 + v_\Delta^2 q_y^2} + (q_x \rightarrow q_y), \quad (9)$$

$$\Pi^{\tau_z}(\mathbf{q}, \epsilon) = \frac{1}{16v_F v_\Delta} \frac{\epsilon^2 + v_\Delta^2 q_y^2}{\sqrt{\epsilon^2 + v_F^2 q_x^2 + v_\Delta^2 q_y^2}} + (q_x \rightarrow q_y), \quad (10)$$

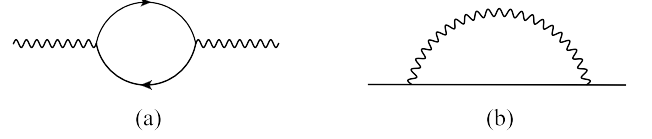


FIG. 3: One-loop corrections due to the Yukawa coupling between nodal QPs and order parameter to: (a) the order-parameter propagator (polarization function) and (b) the fermionic propagator (self-energy), where the solid and wavy lines represent the fermionic and order-parameter propagators, respectively.

for Type- τ_x , Type- τ_y , and Type- τ_z , in tandem with Type- τ_0 that are listed by

$$\Pi_A^{\tau_0}(q_x, q_y, \epsilon) = -\frac{1}{16v_F v_\Delta} \sqrt{\epsilon^2 + v_F^2 q_x^2 + v_\Delta^2 q_y^2}, \quad (11)$$

$$\Pi_B^{\tau_0}(q_y, q_x, \epsilon) = -\frac{1}{16v_F v_\Delta} \sqrt{\epsilon^2 + v_F^2 q_y^2 + v_\Delta^2 q_x^2}. \quad (12)$$

Inserting these polarization functions (8)-(12) into the free order-parameter action (5) by virtue of Dyson equation reformulates the quadratic part of S_{ϕ_0} into [17, 63]

$$[-2(r - r_c) + q^2]\phi_0^2 \rightarrow [-2(r - r_c) + q^2 + \Pi^{\mathcal{M}}(q)]\phi_0^2. \quad (13)$$

At the low-energy regime, one can realize that the term $\Pi^{\mathcal{M}}(q)$ is proportional to q and such additional linear- q term dominates over the q^2 term which henceforth can be neglected [17, 63]. This manifestly indicates that the incorporation of q term qualitatively alters the dynamical nature of the order-parameter action. Additionally, it is the polarization term that substantially modifies the action via involving two significant quantities including the nodal QPs' Fermi velocity v_F and the gap velocity v_Δ . In other words, it is now suitable to designate a renormalized order-parameter field ϕ to replace the bare one. As a result, we are left with the following renormalized order-parameter action

$$S_\phi = \begin{cases} \frac{1}{2} \int \frac{d^3q}{(2\pi)^3} [-2(r - r_c) + \Pi^{\mathcal{M}}(q)]\phi^2, & \mathcal{M} = \tau_j, \end{cases} \quad (14)$$

$$\begin{cases} \frac{1}{2} \sum_{\sigma=A,B} \int \frac{d^3q}{(2\pi)^3} [-2(r - r_c) + \Pi_\sigma^{\mathcal{M}}(q)]\phi_\sigma^2, & \mathcal{M} = \tau_0. \end{cases} \quad (15)$$

And the order-parameter propagator for Type- \mathcal{M} is then given by [11, 17, 18, 48]

$$G_\phi^{\mathcal{M}}(\mathbf{q}, \epsilon) = \frac{1}{\Pi^{\mathcal{M}}(\mathbf{q}, \epsilon)}, \quad (16)$$

as approaching the QCP shown in Fig. 1, where $\mathcal{M} = \tau_{0,x,y,z}$ correspond to the four potential distinct types of phase transitions delivered in Sec. II A. In addition, the Yukawa coupling (3)-(4) between the nodal QPs and order parameter would be accordingly reshaped as

$$\frac{1}{2} \int d^2\mathbf{x} d\tau [\lambda(\phi(\Psi_1^\dagger \mathcal{M} \Psi_1 + \Psi_2^\dagger \mathcal{M} \Psi_2))], \quad \mathcal{M} = \tau_j, \quad (17)$$

$$\frac{1}{2} \int d^2\mathbf{x} d\tau [\lambda(\phi_A \mathcal{M} \Psi_1^\dagger \Psi_1 + \phi_B \mathcal{M} \Psi_2^\dagger \Psi_2)], \quad \mathcal{M} = \tau_0, \quad (18)$$

with the coupling strength λ_0 being also adjusted to λ for consistence.

In order to capture more critical information influenced by the QCP shown in Fig. 1, we hereafter reformulate the nodal QPs' part S_Ψ (2) via supplementing the interaction between nodal QPs themselves dubbed S_{ff} in conjunction with the renormalized order-parameter action (14)-(15) and Yukawa couplings (17)-(18) to establish our effective action as follows,

$$S_{\text{eff}} = S_\Psi + S_\phi + S_{\Psi\phi} + S_{\text{ff}}, \quad (19)$$

where the fermion-fermion interactions S_{ff} is expressed as [69, 104]

$$S_{\text{ff}} = \sum_{i=0}^3 u_i \int d^2\mathbf{x} [\Psi^\dagger(\mathbf{x})\tau_i\Psi(\mathbf{x})]^2, \quad (20)$$

with the indexes $i = 0, 1, 2, 3$ corresponding to four types of fermion-fermion interactions and the parameter u_i measuring their coupling strengths.

Compared to other physical ingredients involved in the phenomenological model, we here would like to address more comments on the fermion-fermion couplings, which as far as we known have not yet been seriously investigated. In the absence of a potential QCP or with the focus on the regions far away from the QCP, it is in principle sensible to drop the fermion-fermion interactions in the superconducting dome of d -wave superconductors as they are known to own a long lifetime and coexist harmoniously with the SC state [31]. In a sharp contrast, as it concerns the question on the critical behaviors neighboring the QCP shown in Fig. 1, we therefore ought to take discreetly into account the contributions from the interplay between the nodal QPs. On one hand, these nodal QPs themselves may mutually intertwine with each other owing to the strong fluctuations and become one of the major elements at the lowest-energy limit [65–79, 81–98, 104]. On the other hand, fermionic couplings can also impact other interaction parameters including fermion velocities $v_{F,\Delta}$ and Yukawa coupling via participating in the coupled RG evolutions, which will be established in Sec. III based upon the strong quantum fluctuations connecting various types of degrees of freedom. In this sense, they can indirectly influence and may play important roles in determining critical behaviors induced by the QCP.

Afterwards, we adopt the effective action (19) as our starting point to derive the coupled flow equations of all associated parameters in the frame of one-loop RG approach [99–101] and explore the physical behaviors of fermion velocities as their effects on superfluid densities and critical temperatures nearby all four types of QCPs illustrated in Fig. 1.

III. RG ANALYSIS

To proceed, we within this section endeavor to perform the one-loop RG analysis [99–101] for our effective

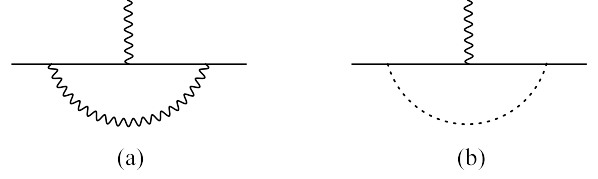


FIG. 4: One-loop corrections to the Yukawa coupling between nodal QPs and order parameter owing to (a) fermion-order parameter interaction and (b) fermion-fermion interaction, where the solid, dashed and wavy lines represent the fermion, fermion-fermion interaction and order parameter, respectively.

action (19) to obtain the coupled RG equations of all interaction parameters, from which the singular properties induced by the QCP are expected to be extracted. To this end, we from now on put our focus on the QCP, namely assuming $r \rightarrow r_c$ in Eq. (19), and then compute all one-loop Feynman diagrams to carry out the standard momentum-shell RG procedures from the field theory perspective.

A. One-loop corrections

We commence with the one-loop corrections to fermionic propagator. As depicted in Fig. 3(b), the free fermionic propagator would receive one-loop corrections $\Sigma^{\mathcal{M}}$, which originates from the Yukawa coupling between the nodal QPs and Type- \mathcal{M} order parameter with $\mathcal{M} = \tau_{0,x,y,z}$. After paralleling the strategy put forward in Refs. [99–101], we integrate out the momentum shell within $b\Lambda - \Lambda$, where Λ is associated with the lattice constant to characterize the cutoff of energy scale and the variable parameter is designated as $b = e^{-l}$ with $l > 0$ being a running energy scale [17–19, 21, 22, 48, 68, 69, 75, 104], and eventually obtain

$$\Sigma^{\tau_x}(\mathbf{k}, \omega) = \lambda^2 [\mathcal{A}_1(-i\omega) + \mathcal{A}_2 v_F k_x \tau^z + \mathcal{A}_3 v_\Delta k_y \tau^x] l, \quad (21)$$

for Type- τ_x order parameter. As to the other three types with $\mathcal{M} = \tau_y, \tau_z, \tau_0$, the structures of their results are analogous to Eq. (21) but the coefficients $\mathcal{A}_{1,2,3}$ are substituted respectively by $\mathcal{B}_{1,2,3}$, $\mathcal{C}_{1,2,3}$, and $\mathcal{D}_{1,2,3}$, whose expressions are presented in Eqs. (A1)-(A4) of Appendix A 1 and Appendix A 2. Accordingly, this gives rise to the renormalized fermionic propagator with the help of the Dyson equation [17, 18, 48],

$$G_\Psi^{-1}(\mathbf{k}, \omega) = -i\omega + v_F k_x \tau^z + v_\Delta k_y \tau^x - \Sigma^{\mathcal{M}}(\mathbf{k}, \omega), \quad (22)$$

where $\Sigma^{\mathcal{M}}(\mathbf{k}, \omega)$ with $\mathcal{M} = \tau_{0,x,y,z}$ specifies the self-energy owing to the Type- \mathcal{M} QPT, which will be one of the critical factors to derive the RG equations.

Next, we take into account the one-loop corrections to the Yukawa coupling and fermion-fermion interactions. At first, we consider the former, which is marginal at the tree level. It is therefore of particular importance to

examine its fate after including the one-loop corrections. To this end, we read off Fig. 4 and realize there exist two sorts of contributions, namely

$$\Xi^{\mathcal{M}} = \Xi_Y^{\mathcal{M}} + \Xi_{\text{ff}}^{\mathcal{M}}, \quad (23)$$

where $\Xi_Y^{\mathcal{M}}$ and $\Xi_{\text{ff}}^{\mathcal{M}}$ with $\mathcal{M} = \tau_{0,x,y,z}$ labeling the Type- \mathcal{M} QPT represent the corrections stemming from order-parameter fluctuations and fermion-fermion interactions, respectively. By borrowing the tactic employed in Refs. [17, 18, 48, 69, 81, 89, 90, 104], we carry out the similarly long but straightforward calculations and finally are left with the following results

$$\Xi_Y^{\mathcal{M}} = \begin{cases} -\mathcal{A}_3 \lambda^3 \tau_x l, & \mathcal{M} = \tau_x, \\ (\mathcal{B}_1 + \mathcal{B}_2 + \mathcal{B}_3) \lambda^3 \tau_y l, & \mathcal{M} = \tau_y, \\ -\mathcal{C}_2 \lambda^3 \tau_z l, & \mathcal{M} = \tau_z, \\ -\mathcal{D}_1^{A,B} \lambda^3 \tau_0 l, & \mathcal{M} = \tau_0, \end{cases} \quad (24)$$

$$(25)$$

$$(26)$$

$$(27)$$

for the order-parameter part and

$$\Xi_{\text{ff}}^{\mathcal{M}} = \begin{cases} \frac{u_2^2 + u_3^2 - u_0^2 - u_1^2}{8\pi v_F v_\Delta} \lambda \tau_x l, & \mathcal{M} = \tau_x, \\ \frac{u_3^2 - u_0^2 - u_2^2}{4\pi v_F v_\Delta} \lambda \tau_y l, & \mathcal{M} = \tau_y, \\ \frac{u_1^2 + u_2^2 - u_0^2 - u_3^2}{8\pi v_F v_\Delta} \lambda \tau_z l, & \mathcal{M} = \tau_z, \end{cases} \quad (28)$$

$$(29)$$

$$(30)$$

fermion-fermion part, respectively.

Then, we turn our focus to the fermion-fermion couplings. In analogy to the Yukawa vertex, both Yukawa couplings and fermion-fermion interactions can contribute to the fermion-fermion vertex dubbed by Γ , which leads to

$$\Gamma^{\mathcal{M}} = \Gamma_Y^{\mathcal{M}} + \Gamma_{\text{ff}}^{\mathcal{M}}, \quad (31)$$

where the indexes \mathcal{M} , Y , and ff share the same meanings with the notations appearing in Eq. (23). We again parallel the approaches adopted in Refs. [67–69, 84, 85, 89, 104] and arrive at the final results, which are attached in Appendix A 1 for convenience.

B. Coupled RG equations

With one-loop corrections in hand, we are now in a suitable position to derive the coupled RG flows of all

interaction parameters that dictate the critical behaviors around the QCP. In the spirit of momentum-shell RG [99–101], we select the quadratic terms of effective action (19) as the “free fixed point” to deliver the RG rescaling transformations of momenta, energy, and fields in the following [17–22, 48, 68, 69, 75, 104]

$$k \rightarrow k' e^{-l}, \quad (32)$$

$$\omega \rightarrow' \omega e^{-l}, \quad (33)$$

$$\Psi_{1,2}(\mathbf{k}, \omega) \rightarrow \Psi'_{1,2}(\mathbf{k}', \omega') e^{\frac{1}{2} \int_0^l (4 - \eta_f) dl}, \quad (34)$$

$$\phi(\mathbf{k}, \omega) \rightarrow \phi'(\mathbf{k}', \omega') e^{\frac{1}{2} \int_0^l (4 - \eta_b) dl}, \quad (35)$$

where the variable parameter $l > 0$ is adopted to specify a running energy scale and delimit the momentum-shell for every RG transformation, which is confined to $b\Lambda - \Lambda$ with Λ specifying a cutoff of energy scale [17, 18, 101]. The anomalous dimensions η_f and η_b are determined by the one-loop corrections in Sec. III A. To one-loop level, we figure out that $\eta_b = 0$ and $\eta_f = -\lambda^2 \mathcal{Z}$ which is inherited from Eq. (22) with $\mathcal{Z} = \mathcal{A}, \mathcal{B}, \mathcal{C}, \mathcal{D}$ for four distinct types of phase transitions classified in Sec. II A.

Subsequently, we gather all one-loop corrections to interaction parameters in Sec. III A and the RG transformation scalings (32)–(35) together to derive the coupled RG equations by carrying out the standard procedures of RG approach [99–101]. In the following, we list the coupled RG equations for Type- τ_x phase transition, consisting of energy-dependent evolutions of fermion velocities and Yukawa coupling,

$$\frac{dv_\Delta}{dl} = \lambda^2 (A_1 - A_3) v_\Delta, \quad (36)$$

$$\frac{dv_F}{dl} = \lambda^2 (A_1 - A_2) v_F, \quad (37)$$

$$\frac{dv_\Delta}{v_F} = \lambda^2 (A_2 - A_3) \frac{v_\Delta}{v_F}, \quad (38)$$

$$\frac{d\lambda}{dl} = \left[A_1 - A_3 + \frac{u_2^2 + u_3^2 - u_0^2 - u_1^2}{8\pi v_F v_\Delta} \right] \lambda^3, \quad (39)$$

as well as fermion-fermion strengths,

$$\frac{du_0}{dl} = \left\{ -1 + 2A_1 - \frac{(u_1 u_2 + u_2 u_3)}{4\pi v_F v_\Delta u_0} + \frac{2\lambda^2}{3} \left[\frac{u_2}{u_0} (A_3 - A_1) - 4A_1 \right] \right\} u_0, \quad (40)$$

$$\frac{du_1}{dl} = \left\{ -1 + 2A_1 + \frac{1}{4\pi v_F v_\Delta} (u_0 - u_1 - u_2 - 2u_3 + \frac{2u_2 u_3}{u_1}) + \frac{2\lambda^2}{3} \left[\frac{u_3}{u_1} (A_3 - A_1) - 4A_3 \right] \right\} u_1, \quad (41)$$

$$\frac{du_2}{dl} = \left\{ -1 + 2A_1 + \frac{1}{4\pi v_F v_\Delta} \left[(2u_0 - 3u_1 - 2u_2 - 3u_3) + \frac{2u_1 u_3}{u_2} \right] + \frac{2\lambda^2}{3} \left[\frac{u_3}{u_2} (A_2 - A_3) + 4A_3 - 5A_1 - 5A_2 \right] \right\} u_2, \quad (42)$$

$$\frac{du_3}{dl} = \left\{ -1 + 2A_1 + \frac{1}{4\pi v_F v_\Delta} \left[(u_0 - u_3 - u_1 - 2u_2) + \frac{2u_1 u_2}{u_3} \right] + \frac{2\lambda^2}{3} \left[\frac{u_2}{u_3} (A_2 - A_3) - A_1 - 5A_2 \right] \right\} u_3. \quad (43)$$

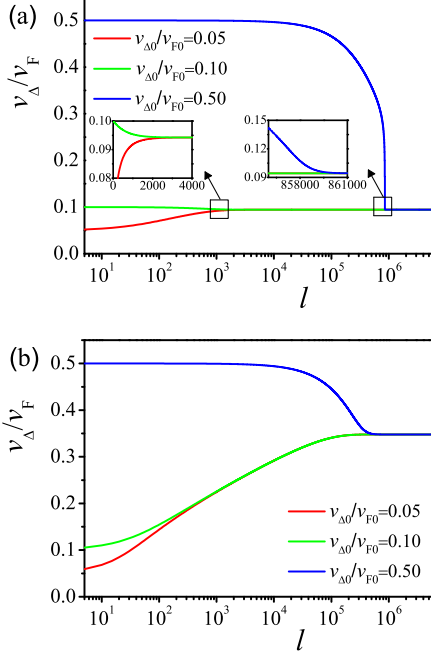


FIG. 5: (Color online) Flows of v_Δ/v_F with decreasing the energy scales (enlarging l) under three representative initial values $v_{\Delta 0}/v_{F0} = 0.05, 0.1, 0.5$ for (a) Type- τ_{0A} and (b) Type- τ_{0B} components of Type- τ_0 QPT at a fixed Yukawa coupling $\lambda = 1$.

In order to make our presentations more compact, we collect and present the related coupled RG equations in Appendix B with respect to the rest three types of phase transitions. Specifically, Eqs. (B1)-(B8) correspond to Type- τ_y , Eqs. (B9)-(B16) to Type- τ_z , and Eqs. (B17)-(B20) to Type- τ_0 , respectively.

In the scenario of RG framework, these evolutions encode intimate entanglements of all interaction parameters [33, 35, 101], which usually enter into the physical implications, and henceforth are expected to be of particular relevance and significance to dictate the low-energy fates of critical properties in the vicinity of certain QCP in Fig. 1. We are about to attentively investigate and address the physical consequences of them in the two looming sections.

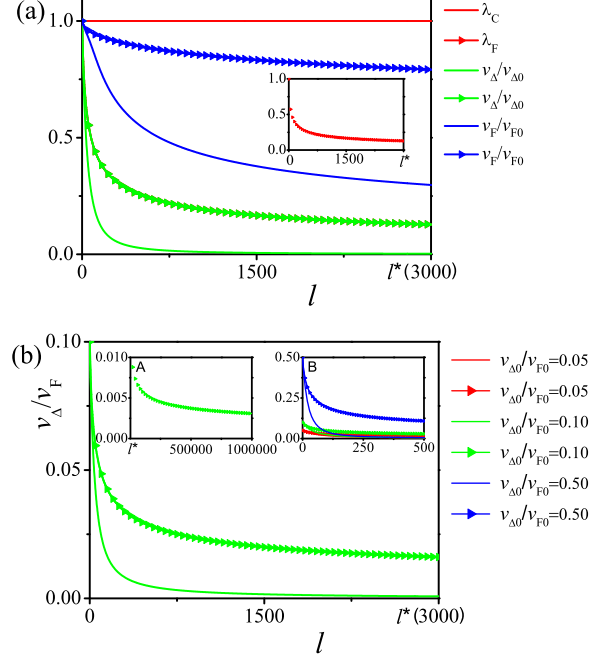


FIG. 6: (Color online) Energy-dependent flows of interaction parameters for both the fixed (bare curves) and flowing (arrowed curves) Yukawa couplings nearby the Type- τ_x QPT (the critical energy scale l^* is designated as the saturated point for $\lambda = 1$ case): (a) evolutions of λ , $v_\Delta/v_{\Delta 0}$, v_F/v_{F0} at a representative initial value $v_{\Delta 0}/v_{F0} = 0.1$ and (b) fates of v_Δ/v_F with Inset A displaying the low-energy limit at $l > l^*$ for the running-coupling case and Inset B presenting its flows at three representative initial values.

IV. LOW-ENERGY BEHAVIORS OF FERMION VELOCITIES

Considering gapless nodal QPs intimately couple with quantum critical fluctuations around certain QPT shown in Fig. 1 [11, 16], two very fermion velocities v_F and v_Δ as well as their ratio v_Δ/v_F would be substantially renormalized. Given the behaviors of fermion velocities are of close relevance to the low-energy physical observables, they are henceforth expected to play an important role in determining the low-energy fates of d -wave superconductors [16, 23–25, 31, 35]. Accordingly, it is of particular importance to inspect the critical behaviors of fermion velocities triggered by the QCP. To this end, we within this section are going to study the energy-dependent coupled RG flow equations addressed in Sec. IIIB, which are assumed to contain the critical information of cer-

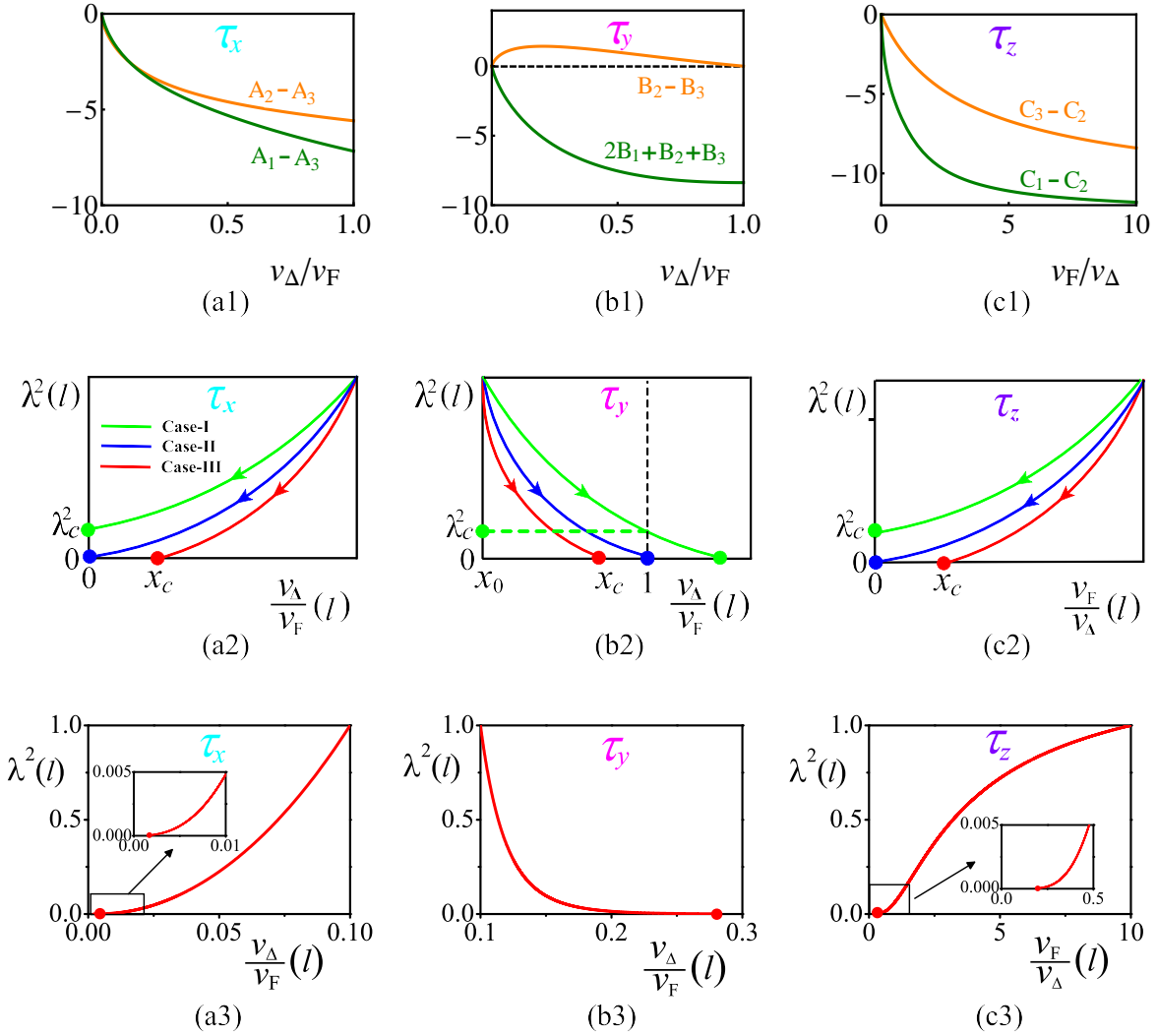


FIG. 7: (Color online) Relationships between the coefficients in RG equations and Yukawa coupling as well as fermion velocities for the potential QPTs. The left column serves as the Type- τ_x QPT: (a1) the v_Δ/v_F dependence of functions $A_1 - A_3$ and $A_2 - A_3$ in Eq. (38)-(39); (a2) three underlying fates of $\lambda^2(l)$ and $\frac{v_\Delta}{v_F}(l)$, which are named as Case-I with $\frac{v_\Delta}{v_F} = 0$ and Case-II with $\lambda^2 = \frac{v_\Delta}{v_F} = 0$ as well as Case-III with $\lambda^2 = 0$; and (a3) the evolution of $\lambda^2(l) - \frac{v_\Delta}{v_F}(l)$ extracted from the coupled RG equations. The middle column denotes the Type- τ_y QPT: (b1) the v_Δ/v_F dependence of functions $2B_1 + B_2 + B_3$ and $B_2 - B_3$ in Eq. (B3)-(B4); (b2) three underlying fates of $\lambda^2(l)$ and $\frac{v_\Delta}{v_F}(l)$, which are dubbed Case-I with $\frac{v_\Delta}{v_F} > 1$, Case-II with $\frac{v_\Delta}{v_F} = 1$ plus Case-III with $\frac{v_\Delta}{v_F} < 1$; and (b3) the evolution of $\lambda^2(l) - \frac{v_\Delta}{v_F}(l)$ extracted from the coupled RG equations. The right column corresponds to the Type- τ_z QPT: (c1) the v_F/v_Δ dependence of functions $C_1 - C_2$ and $C_3 - C_2$ in Eq. (B11)-(B12); (c2) three underlying fates of $\lambda^2(l)$ and $\frac{v_F}{v_\Delta}(l)$, which are classified as Case-I with $\frac{v_F}{v_\Delta} = 0$, Case-II with $\lambda^2 = \frac{v_F}{v_\Delta} = 0$ and Case-III with $\lambda^2 = 0$; and (c3) the evolution of $\lambda^2(l) - \frac{v_F}{v_\Delta}(l)$ extracted from the coupled RG equations.

tain QCP.

A. In the absence of fermion-fermion interactions

Despite both fermion-fermion interactions and quantum fluctuations of order parameters are involved in our RG equations in Sec III, we at first switch off the fermion-fermion interactions to explicitly investigate the effects of all four sorts of order parameters with the reduced cou-

pled RG equations consists of v_F , v_Δ , plus λ , and then defer the contribution from fermionic couplings to next subsection IV B.

1. Fixed Yukawa coupling

As aforementioned in Sec. II, there exist four reduced types of QPTs at r_c , which are schematically shown in Fig. 1 on the basis of the group theory analysis [11-13].

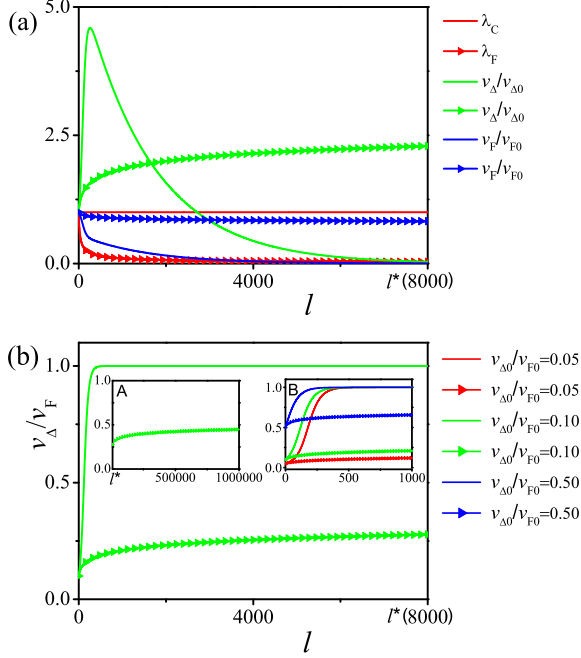


FIG. 8: (Color online) Energy-dependent flows for both the fixed (bare curves) and flowing (arrowed curves) Yukawa couplings nearby the Type- τ_y QPT (the critical energy scale l^* is designated as the saturated point for $\lambda = 1$ case): (a) evolutions of λ , $v_\Delta/v_{\Delta 0}$, $v_F/v_{F 0}$ at a representative initial value $v_{\Delta 0}/v_{F 0} = 0.1$ and (b) fates of v_Δ/v_F with Inset A displaying the low-energy limit at $l > l^*$ for the running-coupling case and Inset B presenting its flows at three representative initial values.

It is worth pointing out that critical behaviors of fermion velocities with approaching the Type- τ_x , $-\tau_y$ or $-\tau_z$ QCP were carefully studied by several researchers in the absence of fermion-fermion interactions [17–20, 22, 38, 48]. In order to simplify the analysis, the Yukawa coupling between nodal QPs and order parameter is regarded as a fixed constant and consequently three distinct fixed points are driven by the quantum criticality, namely $(v_\Delta/v_F)^* \rightarrow 0$ [17], $(v_\Delta/v_F)^* \rightarrow 1$ [48], and $(v_F/v_\Delta)^* \rightarrow 0$ [48] for Type- τ_x , $-\tau_y$ and $-\tau_z$, respectively.

As to Type- τ_0 QPT, it has not yet been seriously investigated to the best of our knowledge. For the sake of completeness, we hereby examine the fate of fermion velocities for such QPT. Learning from the RG analysis in Sec. III B, it is of particular interest to figure out that the Yukawa coupling λ is marginal to one-loop level. In other words, this is equivalent to the situation of fixed Yukawa coupling. Performing numerical evaluation of coupled RG equations for Type- τ_0 QPT (B17)-(B20) gives rise to the main results delineated in Fig. 5. It manifestly shows that the trajectories of v_Δ/v_F with variation of initial values eventually converge to the same finite value at the lowest-energy limit. To be specific, with lowering the energy scale, v_Δ/v_F is attracted by either fixed point

$(v_\Delta/v_F)^* \approx 0.3478$ or $(v_\Delta/v_F)^* \approx 0.0942$, which corresponds to Type- τ_{0A} or Type- τ_{0B} component and is insensitive to initial conditions. As a consequence, Type- τ_0 QPT, in marked contrast to extreme anisotropies caused by its Type- $\tau_{x,z}$ counterparts, prefers to induce some finite anisotropy of fermion velocities.

2. Flowing Yukawa coupling

Compared to the fixed-coupling assumption [17–20, 22, 38, 48, 63, 64], much more physical information would be captured after seriously taking into account the potential evolution of Yukawa coupling λ appearing in Eq. (4). As apparently exhibited in Sec. III B, the coupled RG equations are jointly dictated by both the flow of λ and its entanglement with other interaction parameters. In this context, one can expect that the low-energy properties of fermion velocities may be partially or heavily modified by the evolution of coupling λ around the putative QCP. In order to clarify these intriguing and significant issues, we hereby place our focus on whether and how the tendencies of fermion velocities can be reshaped for all types of QPTs. With respect to the Type- τ_0 QPT, it is worthwhile to highlight that the coupling λ is marginal as depicted in Eq. (B20), indicating an effective fixed-coupling case which is studied in Sec. IV A 1. As to the other three types of QPTs, we subsequently address one by one in the following.

At the outset, we inspect how fermion velocities behave as approaching the Type- τ_x QPT. The corresponding coupled RG evolutions are provided in Eqs. (36)-(39), which are indicative of the close interplay between parameter λ and fermion velocities v_F and v_Δ . After choosing several representative initial conditions to perform numerical calculations, we realize that flowing λ plays an important role in the energy-dependent tendencies of all related parameters as displayed in Fig. 6. Before going further, two helpful points need to be clarified. For the sake of comparison, we from now on would also supplement the corresponding results of fixed-coupling cases with $\lambda = 1$ for simplicity in our numerical results [17–20, 48]. Additionally, a critical energy scale denoted by l^* is designated to serve as the saturated point for $\lambda = 1$ case. Learning from Fig. 6, we find that both v_Δ and v_F for case $\lambda = 1$ rapidly decrease upon lowering the energy scales. In particular, v_Δ falls down more quickly than v_F and thus their ratio v_Δ/v_F goes towards zero at the lowest-energy limit. This implies that v_Δ vanishes but instead v_F still acquires a finite value at $l \geq l^*$. In striking comparison, once the Yukawa coupling is involved in the coupled RG evolutions as well, λ itself gradually descends and evolves towards zero at the lowest-energy limit. As a result, the downtrends of fermion velocities are much slower than their $\lambda = 1$ counterparts. Specifically, both v_Δ and v_F gently decrease and evolve towards finite values at l^* . Concerning their ratio v_Δ/v_F , Fig. 6(b) shows that the extremely anisotropy is broken and replaced by

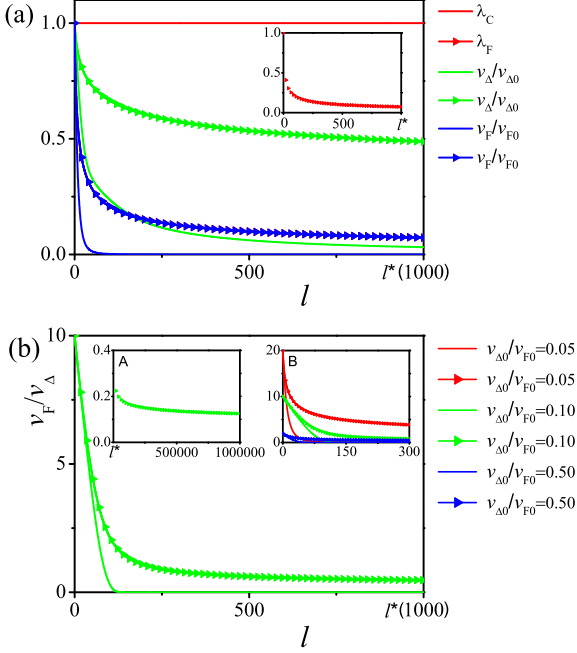


FIG. 9: (Color online) Energy-dependent flows for both the fixed (bare curves) and flowing (arrowed curves) Yukawa couplings nearby the Type- τ_z QPT (the critical energy scale l^* is designated as the saturated point for $\lambda = 1$ case): (a) evolutions of λ , $v_\Delta/v_{\Delta 0}$, v_F/v_{F0} at a representative initial value $v_{\Delta 0}/v_{F0} = 0.1$ and (b) fates of v_F/v_Δ with Inset A displaying the low-energy limit at $l > l^*$ for the running-coupling case and Inset B presenting its flows at three representative initial values.

a finite anisotropy at l^* under the influence of the running coupling λ . Therefore, we come to a conclusion that the low-energy fates of fermion velocities are heavily affected by the participation of energy-dependent λ . In particular, the destruction of extreme anisotropy of v_Δ/v_F would impose a direct or indirect impact on the physical quantities nearby the putative QCP.

Prior to investigating the Type- τ_y QPT, we endeavor to examine the stability of v_Δ/v_F nearby the Type- τ_x QPT at $l = l^*$ and pinpoint its final fate at $l > l^*$. It is manifestly shown in Fig. 6(b) that v_Δ/v_F in the fixed-coupling case is nearly saturated with the extreme anisotropy at the critical energy scale. This is apparent distinction to the running-coupling situation, in which the ratio reduces to certain finite value at $l = l^*$. With an aim to explore the tendency of v_Δ/v_F in the lowest-energy limit, we enlarge the variable $l > l^*$ to obtain the inset A of Fig. 6(b), displaying that the ratio is still unsaturate. In light of the technical deficiency of numerical evaluation, it seems unrealistic to determine whether v_Δ/v_F vanishes or reaches a finite value at $l \rightarrow \infty$. As a consequence, we resort to tentatively analytical analysis of RG equations in association with the numerical results. In principle, the behavior of v_Δ/v_F is directly

determined by the coefficients in Eq. (38) including λ^2 and $A_2 - A_3$. Each of them going towards zero hints to the stop of RG flow with a stable v_Δ/v_F . Once the coupling λ goes towards zero before the latter, the ratio v_Δ/v_F can either be a finite value or zero. However, it is worth emphasizing that the vanishment of $A_2 - A_3$ is tantamount to $v_\Delta/v_F = 0$ as delineated in Fig. 7(a1). Accordingly, as illustrated in Fig. 7(a2), there are three distinct circumstances in all for the ratio of fermion velocities at the lowest-energy limit, which correspond to Case-I with $\lambda^2 \neq 0$ and Case-II with $\lambda^2 = v_\Delta/v_F = 0$ as well as Case-III with $v_\Delta/v_F \neq 0$. With the help of numerical results, Fig. 7(a3) recapitulates the tendencies of λ^2 and v_Δ/v_F with decreasing the energy scale. On the basis of these, we figure out that Case-III is selected by the coupled RG evolutions and hence v_Δ/v_F for Type- τ_x QPT is eventually attracted by a finite fixed point at the lowest-energy limit. This is consistent with the previous analysis at $l \leq l^*$ and therefore hints to the destruction of extreme anisotropy of fermion velocities due to the evolution of Yukawa coupling.

Subsequently, we move to examine the low-energy fates of fermion velocities as accessing the Type- τ_y QPT. Initially, let us aim at the regime $l \in [0, l^*]$ in which the numerical results of the associated RG equations are provided in Fig. 8. As for the fixed-coupling $\lambda = 1$ [17–20, 22, 38, 48, 63, 64], it can be seen from Fig. 8(a) that v_Δ quickly climbs up and then keeps decreasing until it vanishes at $l = l^*$. Meanwhile, v_F monotonically falls down to zero. These make the fermion velocities isotropic with $(v_\Delta/v_F)^* = 1$ at $l = l^*$, which is insensitive to the starting condition as displayed in Fig. 8(b). In sharp contrast, the coupled RG equations (B1)-(B4) force the coupling λ to interact with other parameters and descend with lowering the energy scale. As a result, fermion velocities present distinct behaviors compared to $\lambda = 1$ as approaching the critical energy scale. In Fig. 8(a), v_Δ gradually goes up to certain finite values, but instead v_F decreases to nonzero values. Accordingly, Fig. 8(b) shows that v_Δ/v_F slowly climbs up and flows towards a finite value, which is smaller than $(v_\Delta/v_F)^* = 1$ and susceptible to the initial conditions. This suggests that the evolution of coupling λ prevents fermion velocities being isotropic but rather results in weak anisotropy as accessing the critical energy scale. Next, we go to judge the final fate at $l > l^*$ under the influence of energy-dependent Yukawa coupling in that v_Δ/v_F is not saturate at $l = l^*$ and even a much larger l as shown in Inset A of Fig. 8(b). In analogy with Type- τ_x case, the final fate of v_Δ/v_F for the Type- τ_y QPT depends upon which one of two coefficients $B_2 - B_3$ and λ^2 in Eq. (B3) is driven to fixed point more quickly. To respond this, we realize the fate of $B_2 - B_3 = 0$ amounts to $v_\Delta/v_F = 1$ and then parallel the strategy for Type- τ_x QPT to present three potential circumstances for λ^2 and v_Δ/v_F in Fig. 7(b2), consisting of Case-I with $v_\Delta/v_F > 1$, Case-II with $v_\Delta/v_F = 1$ plus Case-III with $v_\Delta/v_F < 1$. The related numerical analysis of RG equations in Fig. 7(b3) exhibits Case-III

is the dominant situation. This henceforth corroborates the results at $l = l^*$ that fermion velocities are forced to a weak anisotropy due to the contribution from the running Yukawa coupling.

At last, we go to investigate the low-energy behaviors of fermion velocities by virtue of the coupled RG flows (B9)-(B12) nearby Type- τ_z QPT. The major results are presented in Fig. 9, in which the distinctions between fixed-coupling and energy-dependent cases are clearly exhibited. Studying from Fig. 9(a), v_F rapidly drops down and vanishes at $l \approx l^*$ with a fixed $\lambda = 1$, but rather v_Δ progressively descends and tends to a finite value [48, 63, 64]. While the Yukawa coupling λ enters into the RG equations, it becomes energy-dependent and quickly climbs down with lowering the energy scale. This brings significant effects to fermion velocities, driving v_Δ drops much more than that of v_F despite both of them smoothly decrease as the energy scale is decreased. With respect to the ratio of fermion velocities at $l \geq l^*$ in Fig. 9(b), we figure out that v_F/v_Δ bears similarities to v_Δ/v_F approaching the Type- τ_x QPT illustrated in Fig. 9(a). In other words, the extreme anisotropy with $v_F/v_\Delta \rightarrow 0$ at $\lambda = 1$ [48] is sabotaged and replaced with a finite anisotropy by the evolution of coupling λ . By the same token, v_F/v_Δ for Type- τ_z QPT hereby does not saturate at $l = l^*$ as shown in Inset A of Fig. 9(b). In this sense, we follow the previous tactic to identify its final fate, which heavily hinges upon the coefficients λ^2 and $C_3 - C_2 = 0$ in Eqs. (B9)-(B12). In resemblance to the analysis for v_Δ/v_F , $C_3 - C_2 = 0$ points to $v_F/v_\Delta = 0$ and then three distinct fates are diagrammatically illustrated in Fig. 7(c2) including Case-I with $\lambda^2 \neq 0$, Case-II with $v_F/v_\Delta = \lambda^2 = 0$ and Case-III with $v_F/v_\Delta \neq 0$, respectively. In the assistance of numerical evaluation, Fig. 7(c3) shows us that Case-III wins the competition with v_F/v_Δ being governed by a finite value. It therefore signals that the evolution of coupling λ drives the extreme anisotropy $v_F/v_\Delta \rightarrow 0$ into a finite anisotropy at the lowest-energy limit.

B. In the presence of fermion-fermion interactions

As aforementioned in Sec. III, fermion-fermion interactions enter into the coupled RG equations and then may play an important role in the low-energy regime via intimately interacting with quantum fluctuations of order parameters and fermion velocities. Based upon the results in the absence of fermion-fermion interactions, we are now in a suitable position within this subsection to investigate how fermion-fermion interactions impact the behaviors of fermion velocities upon approaching the putative QCPs, which are insufficiently taken into account in previous efforts [17–20, 22, 38, 48, 63, 64].

To achieve this goal, we have to study the coupled RG equations, which consist of v_F , v_Δ , and λ as well as fermion-fermion interactions characterized by u_i with $i = 0, 1, 2, 3$. To proceed, we at first consider the Yukawa

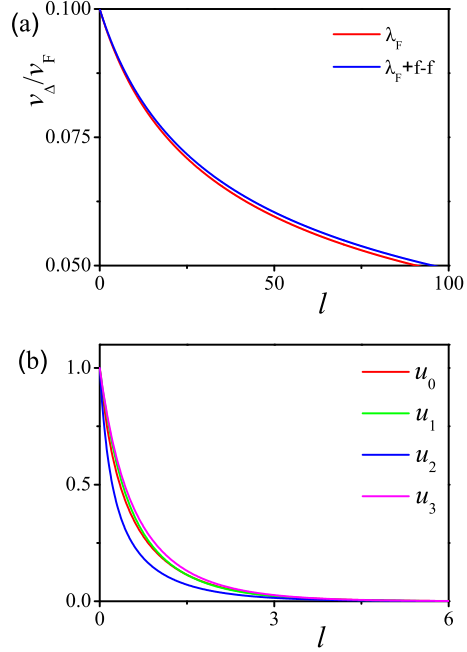


FIG. 10: (Color online) Effects of fermion-fermion interactions for the Type- τ_x QPT on (a) the behaviors of v_Δ/v_F at an initial value $v_{\Delta 0}/v_{F0} = 0.1$ (λ_F and $\lambda_F + f-f$ correspond to the absence and presence of fermion-fermion interactions, respectively), and (b) the energy-dependent evolutions of fermion-fermion interaction strengths $u_{0,1,2,3}$ (the basic tendencies for Type- $\tau_{y,z}$ QPTs are similar and hence not shown here).

fixed-coupling case [17–20, 48]. Learning from the RG equations of fermion velocities (36)-(38), we can infer that the fermion-fermion interactions u_i cannot directly affect v_F and v_Δ , but rather only indirectly modify them via entangling with the interaction parameter λ . In other words, the fermion velocities would receive the contributions from fermion-fermion interactions once the coupling λ flows under the RG equations. This implies that the low-energy properties of fermion velocities for the fixed-coupling situation are adequately robust against fermion-fermion interactions. Next, our focus is moved to the situation with the energy-dependent evolution of Yukawa-coupling λ . After carrying out the numerical analysis of coupled RG equations (36)-(43), we present the comparison between the absence and presence of fermion-fermion interactions in Fig. 10(a) as approaching the Type- τ_x QPT. It can be seen from Fig. 10(a) that the ratio of fermion velocities v_Δ/v_F under fermion-fermion interactions shares the same downtrend with its behaviors in the absence of fermion-fermion interactions. However, one can unambiguously realize that fermion-fermion interactions do bring considerable quantitative effects, which are in favor of retarding the v_Δ/v_F 's decrease as the energy scale is lowered. These are consistent with the fact exhibited in Fig. 10(b) that the fermion-fermion interactions u_i with $i = 0, 1, 2, 3$ are all irrelevant to one-loop level,

which become less and less important as the energy scale is decreased [102]. Paralleling above analysis to Type- $\tau_{y,z}$ QPTs gives rise to the qualitative agreements with their Type- τ_x 's counterpart. As a consequence, the fermion-fermion interactions would provide non-ignorable contributions to the fermion velocities in the vicinity of a putative QPT although they do not play a crucial role compared to the quantum fluctuations of order parameters.

Before closing this section, a brief summary is delivered as follows. With the help of coupled RG equations around the putative QPTs, we systematically investigate the effects of quantum fluctuations and fermion-fermion interactions on the low-energy behaviors of fermion velocities and potential fixed points at the lowest-energy limit. On one hand, we turn off the fermion-fermion interactions and then notice that there exist two fixed points of v_Δ/v_F for Type- τ_0 QPT, which are independent upon the evolution of Yukawa coupling. In sharp comparison, the fixed points for Type- $\tau_{x,y,z}$ QPTs derived at a fixed-coupling $\lambda = 1$ [17, 48] are seriously modified whilst the Yukawa coupling is involved in the coupled RG equations. To be specific, the extreme anisotropy of fermion velocities for Type- $\tau_{x,z}$ is broken and replaced by some finite anisotropy. As to the Type- τ_y QPT, the evolution of coupling λ drives the isotropic system into a finite anisotropic fixed point. On the other hand, we find that the fates of fermion velocities are principally robust against the fermion-fermion interactions although certain quantitative effects are generated to retard the tendencies flowing towards potential fixed points. Subsequently, it is ready to examine the consequences of these unusual behaviors of fermion velocities on the quantum criticality of physical observables.

V. SUPERFLUID DENSITY AND CRITICAL TEMPERATURE

Quantum criticality of fermion velocities around a putative QCP is carefully studied and detailedly addressed in the previous section IV after simultaneously collecting the quantum fluctuations of order parameters and fermion-fermion interactions. In order to present these unique behaviors of fermion velocities that are inconvenient to be detected directly, one can resort to examining the low-energy physical observables in that the fermion velocities plus their ratio v_Δ/v_F usually enter into the physical quantities and play an important role in the low-energy regime [31, 45, 49–52]. This therefore provides us a useful routine to study the distinctions among different QPTs and the very positions of QCPs.

For this purpose, we within this section concentrate on the properties of superfluid density and critical temperature upon accessing the QCPs [19, 20, 22, 48, 50, 103–105], which are two of the most key quantities of superconductors. In order to simplify our analysis, the effects of fermion-fermion interactions are hereafter not considered since they are always subordinate to the Yukawa

couplings between nodal QPs and order parameters [102] and hence cannot alter the basic results caused by the quantum fluctuations as discussed in Sec. IV B. Rather, we primarily try to examine how these two quantities behave under distinct fates of fermion velocities with approaching the assumed QCPs which are induced by the fermion-order parameter couplings and explicitly presented in Sec. IV A.

A. Superfluid density and critical temperature nearby the QCP

Generally, the zero-temperature superfluid density of d -wave superconductor in underdoped region depends linearly on doping concentration x and can be written as [106, 107]

$$\rho^s(0) = \frac{x}{a^2}, \quad (44)$$

where a stands for the lattice spacing constant. To proceed, it is inevitable that a certain amount of normal nodal QPs would be thermally excited out from the SC condensate at a finite temperature, which can efficiently deplete the superfluid density [50]. As a result, the temperature-dependent superfluid density can be expressed as [50]

$$\rho^s(T) = \rho^s(0) - \rho^n(T), \quad (45)$$

where $\rho^s(T)$ and $\rho^n(T)$ serve as the superfluid density and normal QPs density at $T > 0$, respectively [38, 48, 50, 103]. In the non-interacting situation, the normal QPs density exhibits a linear temperature dependence [107] and takes the form of [50]

$$\rho^n(T) = m \frac{2 \ln 2}{\pi} \frac{v_F}{v_\Delta} T, \quad (46)$$

with the parameter m being the mass of nodal QP. This implies that the superfluid density decreases as the temperature is lifted. In such scenario, the critical temperature can be explicitly derived via assuming $\rho^s(T) = 0$ at T_c ,

$$T_c = \frac{1}{2 \ln 2} \frac{v_\Delta}{v_F} \frac{x}{ma^2}, \quad (47)$$

which is well consistent with the Uemura plot [108]. This indicates T_c is readily obtained for the region away from the QCPs, in which the ratio of fermion velocities for noninteracting nodal QPs takes a constant, for instance $v_\Delta/v_F \approx 0.1$ for $\text{YBa}_2\text{Cu}_3\text{O}_{6+\delta}$ [31, 109].

In comparison, the involved physics is much more complicated but rather interesting in the vicinity of certain QCP depicted in Fig. 1. As systematically addressed in Sec IV, the fermion velocities v_F and v_Δ as well as other interaction parameters in the effective theory with approaching the QCPs are heavily renormalized by ferocious quantum fluctuations and become

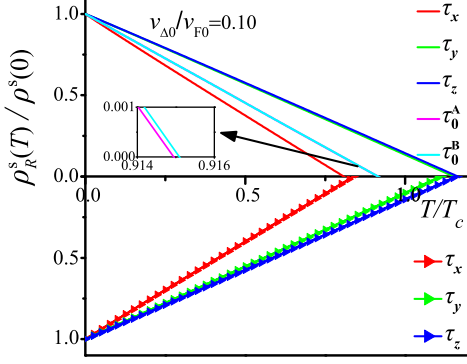


FIG. 11: (Color online) The renormalized superfluid densities and critical temperatures in the vicinity of Type- $\tau_{x,y,z,0}$ QCPs for both the fixed Yukawa coupling (bare lines) and energy-dependent λ (arrowed lines) cases at a representative initial value $v_{\Delta 0}/v_{F0} = 0.1$. Hereby, T_c denotes the critical temperature in the absence of any QCP and the basic results are independent of the initial conditions as depicted in Fig. 13.

energy-dependent under the control of the coupled RG equations in Sec. III B. It is worth emphasizing that the ratio of fermion velocities, which is directly related to the superfluid density as delineated in Eq. 46, exhibits a cornucopia of energy-dependent behaviors and flows towards several fixed points at the lowest-energy limit. With these respects, in order to capture the effects of quantum criticality, we take into account the renormalized fermion velocities and follow the approach in Refs. [38, 48–50, 103] to construct the following renormalized normal QPs density,

$$\rho_R^n(T) = \frac{4m}{k_B T} \int^\Lambda \frac{d^2 \mathbf{k}}{(2\pi)^2} \frac{v_F^2(k) e^{\frac{\sqrt{v_F^2(k)k_x^2 + v_\Delta^2(k)k_y^2}}{k_B T}}}{\left(1 + e^{\frac{\sqrt{v_F^2(k)k_x^2 + v_\Delta^2(k)k_y^2}}{k_B T}}\right)^2}, \quad (48)$$

where k_B denotes the Boltzmann constant and $v_{\Delta,F}$ are dictated by associated RG equations in Sec. III B. This henceforth yields to the renormalized superfluid density

$$\rho_R^s(T) = \rho^s(0) - \rho_R^n(T), \quad (49)$$

from which the renormalized critical temperature can be derived via taking $\rho_R^s(T) = 0$ at $T = T_c$.

As a consequence, Eq. (48) together with Eq. (49) signal that both superfluid density and critical temperature are intimately associated with the energy-dependent fermion velocities, which are governed by the coupled RG evolutions in Sec. III B and display many peculiar properties for all four sorts of QPTs as presented in Sec. IV. In the rest of this section, we are about to pin down the fates of superfluid density and critical temperature at the lowest-energy limit for all types of QPTs in Fig. 1.

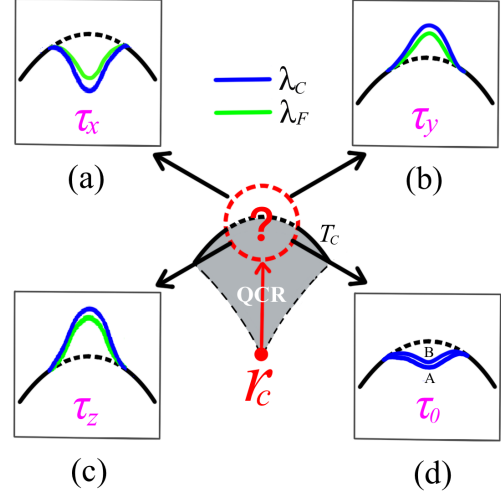


FIG. 12: (Color online) Schematic collections for the fates of critical temperatures caused by quantum fluctuations around the Type- $\tau_{x,y,z,0}$ QCPs as illustrated in Fig. 1 in the absence (λ_C) and presence (λ_F) of evolution of Yukawa coupling.

B. Fates at $v_{\Delta 0}/v_{F0} = 0.1$

On the basis of analysis in Sec. V A, v_Δ/v_F plays a central role in determining the fates of both the superfluid density and critical temperature as explicitly displayed in Eq. (48) and Eq. (49). In order to obtain the energy-dependent v_Δ/v_F , it enables us to fix its initial value and then carry out the numerical evaluation of coupled RG equations in Sec. III B. Without loss of generality, we hereby place our primary focus on the initial condition with $v_{\Delta 0}/v_{F0} = 0.1$ as such ratio appears in most of high- T_c superconductors [16, 31, 109], and then discuss the stability of basic results against the initial conditions in the following subsection.

To proceed, performing the numerical calculations of coupled RG equations for all types of QPTs with such starting condition and inserting them into Eqs. (48)-(49) give rise to the critical behaviors of superfluid density and critical temperature for distinct types of QPTs as collected in Fig. 11, in which the T_c denotes the critical temperature in the absence of a putative QCP. It is noteworthy that the intersections of the curves $\rho_R^s(T)/\rho^s(0)$ with the horizontal axis T/T_c characterize the renormalized critical temperatures after incorporating the quantum criticality of the related QPTs. In addition, given the low-energy tendencies of fermion velocities are of particular difference, we utilize the \tilde{T}_c and \bar{T}_c to specify the critical temperatures for a fixed Yukawa coupling ($\lambda = 1$) and an evolution of λ , respectively. The details are addressed as follows.

At first, we consider the Type- τ_0 QPT. In this case, the Yukawa coupling λ mentioned in Sec. IV A 1 is marginal

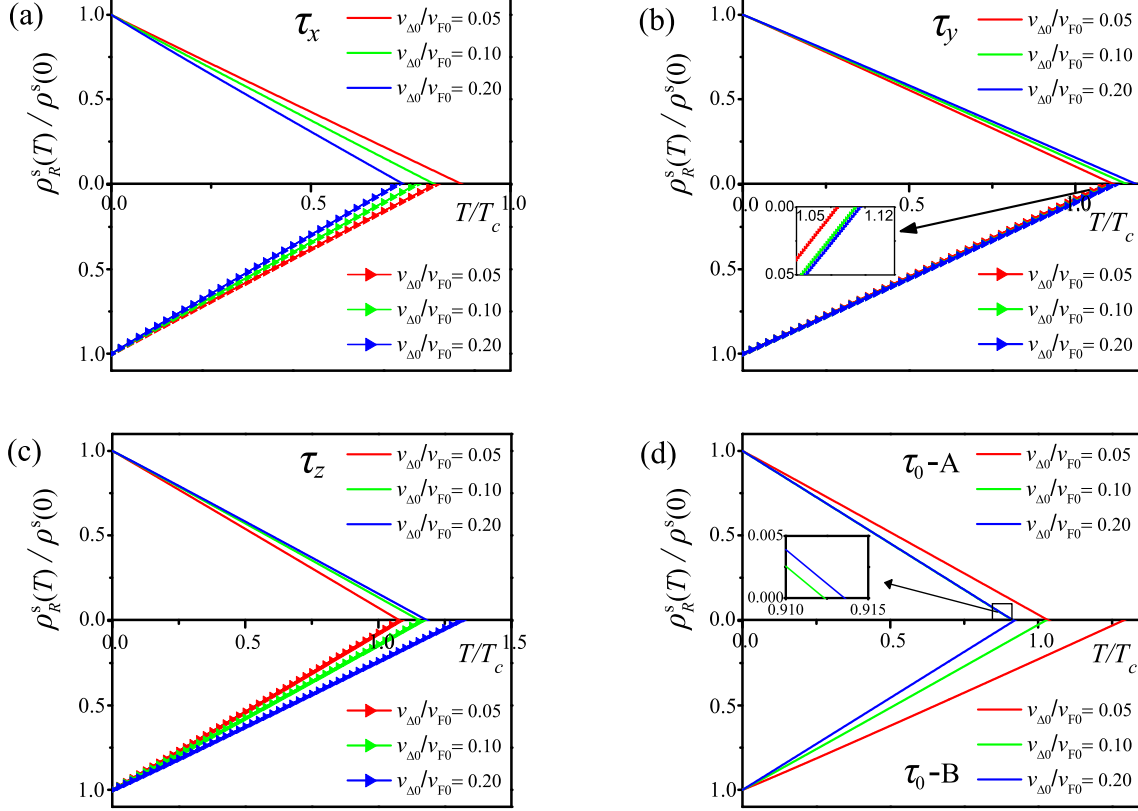


FIG. 13: (Color online) The stabilities of renormalized superfluid densities and critical temperatures against the variation of initial conditions upon approaching (a) Type-\$\tau_x\$, (b) Type-\$\tau_y\$, (c) Type-\$\tau_z\$ and (d) Type-\$\tau_0\$ QPTs for both the fixed Yukawa coupling (bare lines) and energy-dependent \$\lambda\$ (arrowed lines) circumstances.

to one-loop level and henceforth it does not evolve with lowering the energy scales. As a result, we only need to take into account the situation with \$\lambda = 1\$. It can be inferred from Fig. 11 that \$\tilde{T}_c^{0A} < \tilde{T}_c^{0B} < T_c\$, which is indicative of the suppression of superconductivity for both the Type-\$\tau_{0A}\$ and Type-\$\tau_{0B}\$ components as schematically illustrated in Fig. 12(d). Next, we turn to the Type-\$\tau_x\$ QPT. In distinction to the Type-\$\tau_0\$ case, \$v_{\Delta}/v_F\$ with a running \$\lambda\$ exhibits very different behaviors compared to its fixed-coupling (\$\lambda = 1\$) counterpart [17] as presented in Sec. IV A 2. In particular, the extreme anisotropy of fermion velocities is broken due to the evolution of Yukawa coupling as shown in Fig. 6. As a result, three sorts of critical temperatures are restricted to follow \$\tilde{T}_c^x < \tilde{T}_c^y < T_c\$ as depicted in Fig. 11. In other words, despite of the suppression of superconductivity, the flowing of \$\lambda\$ as portrayed in Fig. 12(a) prefers to hinder the decrease of critical temperature. At last, let us move to the Type-\$\tau_y\$ and Type-\$\tau_z\$ QPTs, in which the basic tendencies of critical temperatures are analogous owing to the quantum fluctuations. At a fixed coupling \$\lambda = 1\$, fermion velocities are driven to the isotropic situation for Type-\$\tau_y\$ QPT [48] but another extreme anisotropy with

\$v_F/v_{\Delta} \rightarrow 0\$ for Type-\$\tau_z\$ QPT [17]. Accordingly, Fig. 11 presents that these cause a little promotion for superconductivity with \$T_c < \tilde{T}_c^y < \tilde{T}_c^z\$. In comparison, Sec. IV A 2 shows that both the isotropic and extremely anisotropic fermion velocities are destroyed by the evolution of coupling \$\lambda\$ but instead \$v_{\Delta}/v_F\$ are attracted by some finite values at the lowest-energy limit. As a consequence, Fig. 11 displays that critical temperatures of both cases reduce. Although the relationship of \$T_c < \tilde{T}_c^y < \tilde{T}_c^z\$ is preserved, the critical temperature of Type-\$\tau_y\$ QPT falls a little more than that of Type-\$\tau_z\$ QPT as illustrated in Fig. 12(b) and Fig. 12(c).

To recapitulate, we come to a conclusion that the superconductivity is enhanced nearby the Type-\$\tau_y\$ and Type-\$\tau_z\$ QPTs and conversely suppressed in the proximity of the Type-\$\tau_{0A}\$, Type-\$\tau_{0B}\$ and Type-\$\tau_x\$ QPTs. The renormalized critical temperatures under these QPTs in Fig. 1 are followed by \$\tilde{T}_c^z > \tilde{T}_c^y > T_c > \tilde{T}_c^{0B} > \tilde{T}_c^{0A} > \tilde{T}_c^x\$, which are schematically summarized in Fig. 12.

C. Stability of T_c against $v_{\Delta 0}/v_{F0}$

For the sake of completeness, we are now in a suitable position to inspect the stability of conclusions concerning the critical temperatures in Sec. VB under the variation of initial condition $v_{\Delta 0}/v_{F0}$ as approaching distinct types of QPTs. There exist two points behind this issue as follows. Although the final fixed points are considerably insensitive to the starting values of fermion velocities as studied in Sec. IV, one can learn from Eq. (48) and Eq. (49) that critical temperature depends not only upon the contributions from the fixed point but also upon the whole low-energy regime. In addition, the initial value $v_{\Delta 0}/v_{F0}$ is inevitable to be affected by various uncontrollable and unexpected factors in real materials despite of $v_{\Delta 0}/v_{F0} = 0.1$ in most of high- T_c superconductors [16, 31, 109].

To proceed, we select three representative initial values $v_{\Delta 0}/v_{F0} = 0.05, 0.1, 0.2$ to examine whether and how the fates of critical temperatures nearby distinct types of QPTs are renormalized by the initial conditions. In order to achieve this end, we parallel the analogous procedures in Sec. VB with the help of associated RG equations and then obtain the main results collected in Fig. 13. At the first sight, we figure out that the effects caused by the variation of $v_{\Delta 0}/v_{F0}$ on a fixed-coupling $\lambda = 1$ circumstance share the qualitative results with that of the evolution of λ case. To be concrete, the critical temperatures around Type- τ_x and Type- τ_0 QPTs are susceptible to the initial values of v_{Δ}/v_F and present a little downtrends upon the increase of $v_{\Delta 0}/v_{F0}$ albeit the stability for suppression of superconductivity displayed in Fig. 13(a) and Fig. 13(d). In comparison, we can learn from Fig. 13(b) and Fig. 13(c) for Type- τ_y and Type- τ_z QPTs that both of the critical temperatures receives a certain amount of enhancements with tuning up the value of $v_{\Delta 0}/v_{F0}$. Meanwhile, the basic restriction between the bare and renormalized critical temperature with $\hat{T}_c > \bar{T}_c > T_c$ is insensitive to the initial condition. This suggests that both the initial values of fermion velocities and evolution of Yukawa coupling are subordinate to unusual behaviors of the fermion velocities which are crucial to pin down the critical temperatures around the QPT.

To be brief, the fates of critical temperatures are of particular robustness against the initial values of fermion velocities in the proximity of the putative QCPs. In other words, the low-energy properties of the fermion velocities that are the external expressions of quantum criticality triggered by the QPTs play a more significant role than initial condition in determining the superfluid density and critical temperature. Accordingly, these distinct fates of critical temperatures schematically shown in Fig. 12 are closely associated with different sorts of QPTs and henceforth provide a helpful clue to experimentally detect the very QPT and fix its location.

VI. SUMMARY

In summary, we study the low-energy fates of fermion velocities and behaviors of superfluid density as well as critical temperature nearby the putative QPTs in d -wave superconductors, which stem from the topological change of nodal points [11–13]. In order to facilitate the analysis, seven candidates of potential QPTs shown in Fig. 1 cluster into four effective categories, which are designated as the Type- τ_0 , Type- τ_x , Type- τ_y and Type- τ_z QPTs in Sec II [11, 48]. By means of the momentum-shell RG approach [99–101], all primary physical ingredients including quantum fluctuations of order parameters, the couplings between order parameters and nodal QPs, and fermion-fermion interactions can be equally captured and encoded in a set of coupled RG equations after taking into account one-loop corrections in Sec. III B. On the basis of these RG equations, we, with the help of both analytical and numerical evaluations, achieve the main results concerning the fixed points of fermion velocities and related physical quantities in the vicinity of QPTs.

To be concrete, the fermion velocities exhibit a number of critical properties caused by the effects of quantum fluctuations and fermion-fermion interactions, which are expected to be in charge of the low-energy fates around the underlying four types of QPTs. At first, the focus is put on the fermion velocities. Besides three distinct fixed points of fermion velocities obtained at the fixed Yukawa coupling $\lambda = 1$, including $v_{\Delta}/v_F \rightarrow 0$ for Type- τ_x [17], $v_{\Delta}/v_F \rightarrow 1$ for Type- τ_y [48], $v_F/v_{\Delta} \rightarrow 0$ for Type- τ_z [48], it is of particular interest to point out that a series of new fixed points are generated due to the interplay between evolution of Yukawa coupling λ together with other interaction parameters. As for the Type- τ_0 QPT, we notice that the ratio of fermion velocities is attracted by either fixed point $(v_{\Delta}/v_F)^* \approx 0.3478$ or $(v_{\Delta}/v_F)^* \approx 0.0942$, which corresponds to Type- τ_{0A} or Type- τ_{0B} component and is insensitive to initial conditions. In comparison, the fixed points for Type- $\tau_{x,y,z}$ QPTs at a fixed-coupling $\lambda = 1$ [17, 48] are manifestly reshaped. Two kinds of extreme anisotropies of fermion velocities for Type- $\tau_{x,z}$ QPTs are both broken and replaced by finite anisotropies. Meanwhile, the isotropic fermion velocities for Type- τ_y QPT are driven to a finite anisotropic fixed point by the evolution of coupling λ . This indicates that fermion velocities prefer to flow towards a finite anisotropy as approaching a putative QPT. In addition to these results caused by the evolution of Yukawa coupling λ , we examine the effects of fermion-fermion interactions on fermion velocities as well, which have not yet been considered seriously. Despite they are subordinate to the quantum fluctuations of order parameters [102], it is noteworthy that the fermion-fermion interactions as shown in Fig. 10 can bring non-ignorable quantitative contributions to the fermion velocities in the vicinity of a putative QPT. Next, both of superfluid density and critical temperature, which are two of the most important observables for superconductors, are carefully investigated

under the unconventional behaviors of fermion velocities around all potential QPTs. Concretely, after combining the expressions of these two observables that are dependent upon the fermion velocities and the coupled RG equations of all interaction parameters, we notice that the renormalized critical temperatures are restricted by $\bar{T}_c^z > \bar{T}_c^y > T_c > \bar{T}_c^{0B} > T_c^{0A} > \bar{T}_c^x$ as schematically illustrated in Fig. 12 for all types of QPTs. In other words, both Type- τ_y and Type- τ_z QPTs are in favor of the superconductivity but rather the critical temperature is suppressed by Type- τ_{0A} , Type- τ_{0B} and Type- τ_x QPTs. In addition, we check that the fates of critical temperatures are primarily determined by unusual behaviors of the fermion velocities and considerably robust against the initial values of fermion velocities.

Our results systematically account for the quantum criticality of both fermion velocities and critical temperatures under the competition among quantum fluctuations and interplay between nodal QPs and order parameters as well as the fermion-fermion interactions near all potential QPTs in d -wave superconductors. In particular, an underlying strategy is provided to experimentally seek the putative QPTs and locate their very positions by virtue of qualitatively distinct behaviors nearby different types of QPTs. We anticipate that these results would be instructive to improve our understandings of the quantum criticality and structure of phase diagram in the d -wave superconductors.

ACKNOWLEDGEMENTS

X.Y.R. thanks J. -Q. Li and W. -H. Bian for the helpful discussions. J.W. is partially supported by the National

Natural Science Foundation of China under Grant No. 11504360.

Appendix A: One-loop corrections for Type- τ_y , τ_z , and τ_0

1. Self energy and vertex

One-loop self energy as shown in Fig. 3(b) receives the corrections from the interplay between the nodal QPs and Type- \mathcal{M} order parameter with $\mathcal{M} = \tau_{0,x,y,z}$ illustrated in Fig. 1. To be compact, we have just presented Type- τ_x in Eq. 21 of Sec III A. In the following, the rest three types are collected after integrating out the momentum shell within $b\Lambda - \Lambda$ [17–19, 21, 22, 48, 68, 69, 75, 104],

$$\Sigma^{\tau_y}(\mathbf{k}, \omega) = \lambda^2 [\mathcal{B}_1(-i\omega) + \mathcal{B}_2 v_F k_x \tau^z + \mathcal{B}_3 v_\Delta k_y \tau^x] l, \quad (\text{A1})$$

$$\Sigma^{\tau_z}(\mathbf{k}, \omega) = \lambda^2 [\mathcal{C}_1(-i\omega) + \mathcal{C}_2 v_F k_x \tau^z + \mathcal{C}_3 v_\Delta k_y \tau^x] l, \quad (\text{A2})$$

$$\Sigma_A^{\tau_0}(\mathbf{k}, \omega) = \lambda^2 [\mathcal{D}_1^A(-i\omega) + \mathcal{D}_2^A v_F k_x \tau^z + \mathcal{D}_3^A v_\Delta k_y \tau^x] l, \quad (\text{A3})$$

$$\Sigma_B^{\tau_0}(\mathbf{k}, \omega) = \lambda^2 [\mathcal{D}_1^B(-i\omega) + \mathcal{D}_2^B v_F k_x \tau^z + \mathcal{D}_3^B v_\Delta k_y \tau^x] l, \quad (\text{A4})$$

where the indexes A and B denote the two components for Type- τ_0 .

With respect to the fermion-fermion interactions renormalized by one-loop corrections as depicted in Fig. 14, we only provide the formal expression in Eq. (31) of Sec. III A. To remedy this, the details of the one-loop contributions are listed as follows after practicing the strategy in Refs. [65, 75–77, 79, 81, 83–85, 89–92, 104],

$$\begin{aligned} \Gamma_{u_0}^{\tau_x} &= u_0 \int_{-\infty}^{\infty} \frac{d\omega_1 d\omega_2 d\omega_3}{(2\pi)^3} \int^b \frac{d^2 \mathbf{k}_1 d^2 \mathbf{k}_2 d^2 \mathbf{k}_3}{(2\pi)^6} \Psi_\sigma^\dagger(\omega_1, \mathbf{k}_1) \tau_0 \Psi_\sigma(\omega_2, \mathbf{k}_2) \Psi_{\sigma'}^\dagger(\omega_3, \mathbf{k}_3) \tau_0 \Psi_{\sigma'}(\omega_1 + \omega_2 - \omega_3, \mathbf{k}_1 + \mathbf{k}_2 - \mathbf{k}_3) \\ &\quad \times \left[\frac{-(u_1 u_2 + u_2 u_3)}{4\pi u_0 v_F v_\Delta} + \frac{2\lambda^2}{3} \left(\frac{u_2}{u_0} (\mathcal{A}_3 - \mathcal{A}_1) - 4\mathcal{A}_1 \right) \right] l, \end{aligned} \quad (\text{A5})$$

$$\begin{aligned} \Gamma_{u_1}^{\tau_x} &= u_1 \int_{-\infty}^{\infty} \frac{d\omega_1 d\omega_2 d\omega_3}{(2\pi)^3} \int^b \frac{d^2 \mathbf{k}_1 d^2 \mathbf{k}_2 d^2 \mathbf{k}_3}{(2\pi)^6} \Psi_\sigma^\dagger(\omega_1, \mathbf{k}_1) \tau_1 \Psi_\sigma(\omega_2, \mathbf{k}_2) \Psi_{\sigma'}^\dagger(\omega_3, \mathbf{k}_3) \tau_1 \Psi_{\sigma'}(\omega_1 + \omega_2 - \omega_3, \mathbf{k}_1 + \mathbf{k}_2 - \mathbf{k}_3) \\ &\quad \times \left[\frac{1}{4\pi v_F v_\Delta} (u_0 - u_1 - u_2 - 2u_3 + \frac{2u_2 u_3}{u_1}) + \frac{2\lambda^2}{3} \left(\frac{u_3}{u_1} (\mathcal{A}_3 - \mathcal{A}_1) - 4\mathcal{A}_3 \right) \right] l, \end{aligned} \quad (\text{A6})$$

$$\begin{aligned} \Gamma_{u_2}^{\tau_x} &= u_2 \int_{-\infty}^{\infty} \frac{d\omega_1 d\omega_2 d\omega_3}{(2\pi)^3} \int^b \frac{d^2 \mathbf{k}_1 d^2 \mathbf{k}_2 d^2 \mathbf{k}_3}{(2\pi)^6} \Psi_\sigma^\dagger(\omega_1, \mathbf{k}_1) \tau_2 \Psi_\sigma(\omega_2, \mathbf{k}_2) \Psi_{\sigma'}^\dagger(\omega_3, \mathbf{k}_3) \tau_2 \Psi_{\sigma'}(\omega_1 + \omega_2 - \omega_3, \mathbf{k}_1 + \mathbf{k}_2 - \mathbf{k}_3) \\ &\quad \times \left\{ \frac{1}{4\pi v_F v_\Delta} \left[(2u_0 - 3u_1 - 2u_2 - 3u_3) + \frac{2u_1 u_3}{u_2} \right] + \frac{2\lambda^2}{3} \left[4\mathcal{A}_3 - 5\mathcal{A}_1 - 5\mathcal{A}_2 + \frac{u_3}{u_2} (\mathcal{A}_2 - \mathcal{A}_3) \right] \right\} l, \end{aligned} \quad (\text{A7})$$

$$\begin{aligned} \Gamma_{u_3}^{\tau_x} &= u_3 \int_{-\infty}^{\infty} \frac{d\omega_1 d\omega_2 d\omega_3}{(2\pi)^3} \int^b \frac{d^2 \mathbf{k}_1 d^2 \mathbf{k}_2 d^2 \mathbf{k}_3}{(2\pi)^6} \Psi_\sigma^\dagger(\omega_1, \mathbf{k}_1) \tau_3 \Psi_\sigma(\omega_2, \mathbf{k}_2) \Psi_{\sigma'}^\dagger(\omega_3, \mathbf{k}_3) \tau_3 \Psi_{\sigma'}(\omega_1 + \omega_2 - \omega_3, \mathbf{k}_1 + \mathbf{k}_2 - \mathbf{k}_3) \\ &\quad \times \left\{ \frac{1}{4\pi v_F v_\Delta} \left[(u_0 - u_3 - u_1 - 2u_2) + \frac{2(u_1 u_2)}{u_3} \right] + \frac{2\lambda^2}{3} \left[\frac{u_2}{u_3} (\mathcal{A}_2 - \mathcal{A}_3) - \mathcal{A}_1 - 5\mathcal{A}_2 \right] \right\} l, \end{aligned} \quad (\text{A8})$$

$$\begin{aligned} \Gamma_{u_0}^{\tau_y} &= u_0 \int_{-\infty}^{\infty} \frac{d\omega_1 d\omega_2 d\omega_3}{(2\pi)^3} \int^b \frac{d^2 \mathbf{k}_1 d^2 \mathbf{k}_2 d^2 \mathbf{k}_3}{(2\pi)^6} \Psi_{\sigma}^{\dagger}(\omega_1, \mathbf{k}_1) \tau_0 \Psi_{\sigma}(\omega_2, \mathbf{k}_2) \Psi_{\sigma'}^{\dagger}(\omega_3, \mathbf{k}_3) \tau_0 \Psi_{\sigma'}(\omega_1 + \omega_2 - \omega_3, \mathbf{k}_1 + \mathbf{k}_2 - \mathbf{k}_3) \\ &\quad \times \left[\frac{-(u_1 u_2 + u_2 u_3)}{4\pi u_0 v_F v_{\Delta}} + \frac{2\lambda^2}{3} \left(-4\mathcal{B}_1 - \frac{u_1}{u_0}(\mathcal{B}_1 + \mathcal{B}_2) + \frac{u_2}{u_0}(\mathcal{B}_2 + \mathcal{B}_3) - \frac{u_3}{u_0}(\mathcal{B}_1 + \mathcal{B}_2) \right) \right] l, \end{aligned} \quad (\text{A9})$$

$$\begin{aligned} \Gamma_{u_1}^{\tau_y} &= u_1 \int_{-\infty}^{\infty} \frac{d\omega_1 d\omega_2 d\omega_3}{(2\pi)^3} \int^b \frac{d^2 \mathbf{k}_1 d^2 \mathbf{k}_2 d^2 \mathbf{k}_3}{(2\pi)^6} \Psi_{\sigma}^{\dagger}(\omega_1, \mathbf{k}_1) \tau_1 \Psi_{\sigma}(\omega_2, \mathbf{k}_2) \Psi_{\sigma'}^{\dagger}(\omega_3, \mathbf{k}_3) \tau_1 \Psi_{\sigma'}(\omega_1 + \omega_2 - \omega_3, \mathbf{k}_1 + \mathbf{k}_2 - \mathbf{k}_3) \\ &\quad \times \left[\frac{1}{4\pi v_F v_{\Delta}} (u_0 - u_1 - u_2 - 2u_3 + \frac{2u_2 u_3}{u_1}) + \frac{2\lambda^2}{3} \left(\frac{u_3}{u_1}(\mathcal{B}_2 + \mathcal{B}_3) - 4\mathcal{B}_3 \right) \right] l, \end{aligned} \quad (\text{A10})$$

$$\begin{aligned} \Gamma_{u_2}^{\tau_y} &= u_2 \int_{-\infty}^{\infty} \frac{d\omega_1 d\omega_2 d\omega_3}{(2\pi)^3} \int^b \frac{d^2 \mathbf{k}_1 d^2 \mathbf{k}_2 d^2 \mathbf{k}_3}{(2\pi)^6} \Psi_{\sigma}^{\dagger}(\omega_1, \mathbf{k}_1) \tau_2 \Psi_{\sigma}(\omega_2, \mathbf{k}_2) \Psi_{\sigma'}^{\dagger}(\omega_3, \mathbf{k}_3) \tau_2 \Psi_{\sigma'}(\omega_1 + \omega_2 - \omega_3, \mathbf{k}_1 + \mathbf{k}_2 - \mathbf{k}_3) \\ &\quad \times \left\{ \frac{1}{4\pi v_F v_{\Delta}} \left[(2u_0 - 3u_1 - 2u_2 - 3u_3) + \frac{2u_1 u_3}{u_2} \right] + \frac{2\lambda^2}{3} \left[4(\mathcal{B}_1 + \mathcal{B}_2 + \mathcal{B}_3) - \frac{u_1}{u_2}(\mathcal{B}_1 + \mathcal{B}_2) - \frac{u_3}{u_2}(\mathcal{B}_1 + \mathcal{B}_3) \right] \right\} l, \end{aligned} \quad (\text{A11})$$

$$\begin{aligned} \Gamma_{u_3}^{\tau_y} &= u_3 \int_{-\infty}^{\infty} \frac{d\omega_1 d\omega_2 d\omega_3}{(2\pi)^3} \int^b \frac{d^2 \mathbf{k}_1 d^2 \mathbf{k}_2 d^2 \mathbf{k}_3}{(2\pi)^6} \Psi_{\sigma}^{\dagger}(\omega_1, \mathbf{k}_1) \tau_3 \Psi_{\sigma}(\omega_2, \mathbf{k}_2) \Psi_{\sigma'}^{\dagger}(\omega_3, \mathbf{k}_3) \tau_3 \Psi_{\sigma'}(\omega_1 + \omega_2 - \omega_3, \mathbf{k}_1 + \mathbf{k}_2 - \mathbf{k}_3) \\ &\quad \times \left\{ \frac{1}{4\pi v_F v_{\Delta}} \left[(u_0 - u_3 - u_1 - 2u_2) + \frac{2(u_1 u_2)}{u_3} \right] + \frac{2\lambda^2}{3} \left[\frac{u_1}{u_3}(\mathcal{B}_2 + \mathcal{B}_3) - 4\mathcal{B}_2 \right] \right\} l, \end{aligned} \quad (\text{A12})$$

$$\begin{aligned} \Gamma_{u_0}^{\tau_z} &= u_0 \int_{-\infty}^{\infty} \frac{d\omega_1 d\omega_2 d\omega_3}{(2\pi)^3} \int^b \frac{d^2 \mathbf{k}_1 d^2 \mathbf{k}_2 d^2 \mathbf{k}_3}{(2\pi)^6} \Psi_{\sigma}^{\dagger}(\omega_1, \mathbf{k}_1) \tau_0 \Psi_{\sigma}(\omega_2, \mathbf{k}_2) \Psi_{\sigma'}^{\dagger}(\omega_3, \mathbf{k}_3) \tau_0 \Psi_{\sigma'}(\omega_1 + \omega_2 - \omega_3, \mathbf{k}_1 + \mathbf{k}_2 - \mathbf{k}_3) \\ &\quad \times \left[\frac{-(u_1 u_2 + u_2 u_3)}{4\pi u_0 v_F v_{\Delta}} + \frac{2\lambda^2}{3} \left(\frac{u_2}{u_0}(\mathcal{C}_2 - \mathcal{C}_1) - 4\mathcal{C}_1 \right) \right] l, \end{aligned} \quad (\text{A13})$$

$$\begin{aligned} \Gamma_{u_1}^{\tau_z} &= u_1 \int_{-\infty}^{\infty} \frac{d\omega_1 d\omega_2 d\omega_3}{(2\pi)^3} \int^b \frac{d^2 \mathbf{k}_1 d^2 \mathbf{k}_2 d^2 \mathbf{k}_3}{(2\pi)^6} \Psi_{\sigma}^{\dagger}(\omega_1, \mathbf{k}_1) \tau_1 \Psi_{\sigma}(\omega_2, \mathbf{k}_2) \Psi_{\sigma'}^{\dagger}(\omega_3, \mathbf{k}_3) \tau_1 \Psi_{\sigma'}(\omega_1 + \omega_2 - \omega_3, \mathbf{k}_1 + \mathbf{k}_2 - \mathbf{k}_3) \\ &\quad \times \left[\frac{1}{4\pi v_F v_{\Delta}} (u_0 - u_1 - u_2 - 2u_3 + \frac{2u_2 u_3}{u_1}) + \frac{2\lambda^2}{3} \left(\frac{u_2}{u_1}(\mathcal{C}_3 - \mathcal{C}_2) - \mathcal{C}_1 - 5\mathcal{C}_3 \right) \right] l, \end{aligned} \quad (\text{A14})$$

$$\begin{aligned} \Gamma_{u_2}^{\tau_z} &= u_2 \int_{-\infty}^{\infty} \frac{d\omega_1 d\omega_2 d\omega_3}{(2\pi)^3} \int^b \frac{d^2 \mathbf{k}_1 d^2 \mathbf{k}_2 d^2 \mathbf{k}_3}{(2\pi)^6} \Psi_{\sigma}^{\dagger}(\omega_1, \mathbf{k}_1) \tau_2 \Psi_{\sigma}(\omega_2, \mathbf{k}_2) \Psi_{\sigma'}^{\dagger}(\omega_3, \mathbf{k}_3) \tau_2 \Psi_{\sigma'}(\omega_1 + \omega_2 - \omega_3, \mathbf{k}_1 + \mathbf{k}_2 - \mathbf{k}_3) \\ &\quad \times \left\{ \frac{1}{4\pi v_F v_{\Delta}} \left[(2u_0 - 3u_1 - 2u_2 - 3u_3) + \frac{2u_1 u_3}{u_2} \right] + \frac{2\lambda^2}{3} \left[4\mathcal{C}_2 - 5\mathcal{C}_1 - 5\mathcal{C}_3 + \frac{u_1}{u_2}(\mathcal{C}_3 - \mathcal{C}_2) \right] \right\} l, \end{aligned} \quad (\text{A15})$$

$$\begin{aligned} \Gamma_{u_3}^{\tau_z} &= u_3 \int_{-\infty}^{\infty} \frac{d\omega_1 d\omega_2 d\omega_3}{(2\pi)^3} \int^b \frac{d^2 \mathbf{k}_1 d^2 \mathbf{k}_2 d^2 \mathbf{k}_3}{(2\pi)^6} \Psi_{\sigma}^{\dagger}(\omega_1, \mathbf{k}_1) \tau_3 \Psi_{\sigma}(\omega_2, \mathbf{k}_2) \Psi_{\sigma'}^{\dagger}(\omega_3, \mathbf{k}_3) \tau_3 \Psi_{\sigma'}(\omega_1 + \omega_2 - \omega_3, \mathbf{k}_1 + \mathbf{k}_2 - \mathbf{k}_3) \\ &\quad \times \left\{ \frac{1}{4\pi v_F v_{\Delta}} \left[(u_0 - u_3 - u_1 - 2u_2) + \frac{2(u_1 u_2)}{u_3} \right] + \frac{2\lambda^2}{3} \left[\frac{u_1}{u_3}(\mathcal{C}_2 - \mathcal{C}_1) - 4\mathcal{C}_2 \right] \right\} l, \end{aligned} \quad (\text{A16})$$

where Eqs. (A5)-(A8) are linked to Type- τ_x , Eqs. (A9)-(A12) to Type- τ_y and Eqs. (A13)-(A16) to τ_z , respectively.

2. Designated coefficients

All related coefficients appearing in both above equations and elsewhere are designated by

$$\mathcal{A}_1 = \frac{2(v_{\Delta}/v_F)}{N_f \pi^3} \int_{-\infty}^{\infty} dx \int_0^{2\pi} d\theta \frac{x^2 - \cos^2 \theta - (v_{\Delta}/v_F)^2 \sin^2 \theta}{[x^2 + \cos^2 \theta + (v_{\Delta}/v_F)^2 \sin^2 \theta]^2} \mathcal{G}_I(x, \theta), \quad (\text{A17})$$

$$\mathcal{A}_2 = \frac{2(v_{\Delta}/v_F)}{N_f \pi^3} \int_{-\infty}^{\infty} dx \int_0^{2\pi} d\theta \frac{[-x^2 + \cos^2 \theta - (v_{\Delta}/v_F)^2 \sin^2 \theta]}{[x^2 + \cos^2 \theta + (v_{\Delta}/v_F)^2 \sin^2 \theta]^2} \mathcal{G}_I(x, \theta), \quad (\text{A18})$$

$$\mathcal{A}_3 = \frac{2(v_{\Delta}/v_F)}{N_f \pi^3} \int_{-\infty}^{\infty} dx \int_0^{2\pi} d\theta \frac{[x^2 + \cos^2 \theta - (v_{\Delta}/v_F)^2 \sin^2 \theta]}{[x^2 + \cos^2 \theta + (v_{\Delta}/v_F)^2 \sin^2 \theta]^2} \mathcal{G}_I(x, \theta), \quad (\text{A19})$$

$$\mathcal{B}_1 = \frac{2(v_{\Delta}/v_F)}{N_f \pi^3} \int_{-\infty}^{\infty} dx \int_0^{2\pi} d\theta \frac{x^2 - \cos^2 \theta - (v_{\Delta}/v_F)^2 \sin^2 \theta}{[x^2 + \cos^2 \theta + (v_{\Delta}/v_F)^2 \sin^2 \theta]^2} \mathcal{G}_{II}(x, \theta), \quad (\text{A20})$$

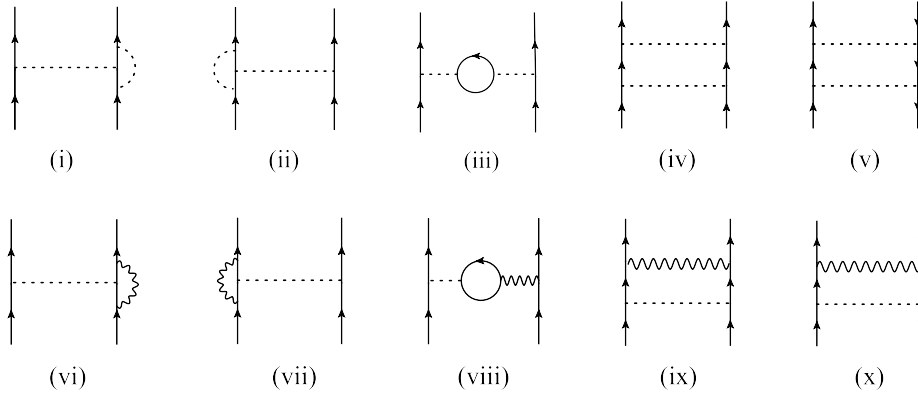


FIG. 14: One-loop corrections to the fermion-fermion interactions due to fermion-fermion interactions (i-v) and Yukawa coupling between nodal fermion and order parameter (vi-x). The solid, dashed and wavy lines represent the fermion propagator, four-fermion interaction and order parameter, respectively.

$$\mathcal{B}_2 = \frac{2(v_\Delta/v_F)}{N_f\pi^3} \int_{-\infty}^{\infty} dx \int_0^{2\pi} d\theta \frac{[-x^2 + \cos^2 \theta - (v_\Delta/v_F)^2 \sin^2 \theta]}{[x^2 + \cos^2 \theta + (v_\Delta/v_F)^2 \sin^2 \theta]^2} \mathcal{G}_{\text{II}}(x, \theta), \quad (\text{A21})$$

$$\mathcal{B}_3 = \frac{2(v_\Delta/v_F)}{N_f\pi^3} \int_{-\infty}^{\infty} dx \int_0^{2\pi} d\theta \frac{[-x^2 - \cos^2 \theta + (v_\Delta/v_F)^2 \sin^2 \theta]}{[x^2 + \cos^2 \theta + (v_\Delta/v_F)^2 \sin^2 \theta]^2} \mathcal{G}_{\text{II}}(x, \theta), \quad (\text{A22})$$

$$\mathcal{C}_1 = \frac{2(v_F/v_\Delta)}{N_f\pi^3} \int_{-\infty}^{\infty} dx \int_0^{2\pi} d\theta \frac{x^2 - \cos^2 \theta - (v_\Delta/v_F)^2 \sin^2 \theta}{[x^2 + \cos^2 \theta + (v_\Delta/v_F)^2 \sin^2 \theta]^2} \mathcal{G}_{\text{III}}(x, \theta), \quad (\text{A23})$$

$$\mathcal{C}_2 = \frac{2(v_F/v_\Delta)}{N_f\pi^3} \int_{-\infty}^{\infty} dx \int_0^{2\pi} d\theta \frac{[x^2 - \cos^2 \theta + (v_\Delta/v_F)^2 \sin^2 \theta]}{[x^2 + \cos^2 \theta + (v_\Delta/v_F)^2 \sin^2 \theta]^2} \mathcal{G}_{\text{III}}(x, \theta), \quad (\text{A24})$$

$$\mathcal{C}_3 = \frac{2(v_F/v_\Delta)}{N_f\pi^3} \int_{-\infty}^{\infty} dx \int_0^{2\pi} d\theta \frac{[-x^2 - \cos^2 \theta + (v_\Delta/v_F)^2 \sin^2 \theta]}{[x^2 + \cos^2 \theta + (v_\Delta/v_F)^2 \sin^2 \theta]^2} \mathcal{G}_{\text{III}}(x, \theta), \quad (\text{A25})$$

$$\mathcal{D}_1^A = \frac{2(v_\Delta/v_F)}{N_f\pi^3} \int_{-\infty}^{\infty} dx \int_0^{2\pi} d\theta \frac{x^2 - \cos^2 \theta - (v_\Delta/v_F)^2 \sin^2 \theta}{[x^2 + \cos^2 \theta + (v_\Delta/v_F)^2 \sin^2 \theta]^2} \mathcal{G}_{\text{IVA}}(x, \theta), \quad (\text{A26})$$

$$\mathcal{D}_2^A = \frac{2(v_\Delta/v_F)}{N_f\pi^3} \int_{-\infty}^{\infty} dx \int_0^{2\pi} d\theta \frac{[x^2 - \cos^2 \theta + (v_\Delta/v_F)^2 \sin^2 \theta]}{[x^2 + \cos^2 \theta + (v_\Delta/v_F)^2 \sin^2 \theta]^2} \mathcal{G}_{\text{IVA}}(x, \theta), \quad (\text{A27})$$

$$\mathcal{D}_3^A = \frac{2(v_\Delta/v_F)}{N_f\pi^3} \int_{-\infty}^{\infty} dx \int_0^{2\pi} d\theta \frac{[x^2 + \cos^2 \theta - (v_\Delta/v_F)^2 \sin^2 \theta]}{[x^2 + \cos^2 \theta + (v_\Delta/v_F)^2 \sin^2 \theta]^2} \mathcal{G}_{\text{IVA}}(x, \theta), \quad (\text{A28})$$

$$\mathcal{D}_1^B = \frac{2(v_\Delta/v_F)}{N_f\pi^3} \int_{-\infty}^{\infty} dx \int_0^{2\pi} d\theta \frac{x^2 - \sin^2 \theta - (v_\Delta/v_F)^2 \cos^2 \theta}{[x^2 + \sin^2 \theta + (v_\Delta/v_F)^2 \cos^2 \theta]^2} \mathcal{G}_{\text{IVB}}(x, \theta), \quad (\text{A29})$$

$$\mathcal{D}_2^B = \frac{2(v_\Delta/v_F)}{N_f\pi^3} \int_{-\infty}^{\infty} dx \int_0^{2\pi} d\theta \frac{[x^2 - \sin^2 \theta + (v_\Delta/v_F)^2 \cos^2 \theta]}{[x^2 + \sin^2 \theta + (v_\Delta/v_F)^2 \cos^2 \theta]^2} \mathcal{G}_{\text{IVB}}(x, \theta), \quad (\text{A30})$$

$$\mathcal{D}_3^B = \frac{2(v_\Delta/v_F)}{N_f\pi^3} \int_{-\infty}^{\infty} dx \int_0^{2\pi} d\theta \frac{[x^2 + \sin^2 \theta - (v_\Delta/v_F)^2 \cos^2 \theta]}{[x^2 + \sin^2 \theta + (v_\Delta/v_F)^2 \cos^2 \theta]^2} \mathcal{G}_{\text{IVB}}(x, \theta), \quad (\text{A31})$$

where the associated functions \mathcal{G}_I , \mathcal{G}_{II} , \mathcal{G}_{III} , \mathcal{G}_{IVA} , and \mathcal{G}_{IVB} are nominated as

$$\mathcal{G}_I^{-1} = \frac{x^2 + \cos^2 \theta}{\sqrt{x^2 + \cos^2 \theta + (v_\Delta/v_F)^2 \sin^2 \theta}} + \frac{x^2 + \sin^2 \theta}{\sqrt{x^2 + \sin^2 \theta + (v_\Delta/v_F)^2 \cos^2 \theta}}, \quad (\text{A32})$$

$$\mathcal{G}_{\text{II}}^{-1} = \sqrt{x^2 + \cos^2 \theta + (v_\Delta/v_F)^2 \sin^2 \theta} + \sqrt{x^2 + \sin^2 \theta + (v_\Delta/v_F)^2 \cos^2 \theta}, \quad (\text{A33})$$

$$\mathcal{G}_{\text{III}}^{-1} = \frac{x^2 + (v_\Delta/v_F)^2 \sin^2 \theta}{\sqrt{x^2 + \cos^2 \theta + (v_\Delta/v_F)^2 \sin^2 \theta}} + \frac{x^2 + (v_\Delta/v_F)^2 \cos^2 \theta}{\sqrt{x^2 + \sin^2 \theta + (v_\Delta/v_F)^2 \cos^2 \theta}}, \quad (\text{A34})$$

$$\mathcal{G}_{\text{IVA}}^{-1} = -\sqrt{x^2 + \cos^2 \theta + (v_\Delta/v_F)^2 \sin^2 \theta}, \quad (\text{A35})$$

$$\mathcal{G}_{\text{IVB}}^{-1} = -\sqrt{x^2 + \sin^2 \theta + (v_\Delta/v_F)^2 \cos^2 \theta}. \quad (\text{A36})$$

Appendix B: Coupled RG equations for Type- τ_y , τ_z , and τ_0

Besides the coupled RG equations for Type- τ_x phase transition exhibited in Eqs. (36)-(43), we perform the standard procedures of momentum-shell RG approach [99–101] and then deliver the corresponding RG evolutions for other types as follows,

$$\frac{dv_F}{dl} = \lambda^2(\mathcal{B}_1 - \mathcal{B}_2)v_F, \quad (\text{B1})$$

$$\frac{dv_\Delta}{dl} = \lambda^2(\mathcal{B}_1 - \mathcal{B}_3)v_\Delta, \quad (\text{B2})$$

$$\frac{d\frac{v_\Delta}{v_F}}{dl} = \lambda^2(\mathcal{B}_2 - \mathcal{B}_3)\frac{v_\Delta}{v_F}, \quad (\text{B3})$$

$$\frac{d\lambda}{dl} = \left[2\mathcal{B}_1 + \mathcal{B}_2 + \mathcal{B}_3 + \frac{[(u_1)^2 + (u_3)^2 - (u_0)^2 - (u_2)^2]}{4\pi v_F v_\Delta} \right] \lambda^3, \quad (\text{B4})$$

$$\frac{du_0}{dl} = \left\{ -1 + 2\mathcal{B}_1 - \frac{(u_1 u_2 + u_2 u_3)}{4\pi v_F v_\Delta u_0} + \frac{2\lambda^2}{3} \left[-4\mathcal{B}_1 - \frac{u_1}{u_0}(\mathcal{B}_1 + \mathcal{B}_3) - \frac{u_3}{u_0}(\mathcal{B}_1 + \mathcal{B}_2) \right] \right\} u_0, \quad (\text{B5})$$

$$\frac{du_1}{dl} = \left\{ -1 + 2\mathcal{B}_1 + \frac{1}{4\pi v_F v_\Delta} (u_0 - u_1 - u_2 - 2u_3 + \frac{2u_2 u_3}{u_1}) + \frac{2\lambda^2}{3} \left[\frac{u_3}{u_1}(\mathcal{B}_2 + \mathcal{B}_3) - 4\mathcal{B}_3 \right] \right\} u_1, \quad (\text{B6})$$

$$\frac{du_2}{dl} = \left\{ -1 + 2\mathcal{B}_1 + \frac{1}{4\pi v_F v_\Delta} \left[(2u_0 - 3u_1 - 2u_2 - 3u_3) + \frac{2u_1 u_3}{u_2} \right] + \frac{2\lambda^2}{3} \left[4(\mathcal{B}_1 + \mathcal{B}_2 + \mathcal{B}_3) - \frac{u_1}{u_2}(\mathcal{B}_1 + \mathcal{B}_2) - \frac{u_3}{u_2}(\mathcal{B}_1 + \mathcal{B}_3) \right] \right\} u_2, \quad (\text{B7})$$

$$\frac{du_3}{dl} = \left\{ -1 + 2\mathcal{B}_1 + \frac{1}{4\pi v_F v_\Delta} \left[(u_0 - u_3 - u_1 - 2u_2) + \frac{2u_1 u_2}{u_3} \right] + \frac{2\lambda^2}{3} \left[\frac{u_1}{u_3}(\mathcal{B}_2 + \mathcal{B}_3) - 4\mathcal{B}_2 \right] \right\} u_3, \quad (\text{B8})$$

for Type- τ_y ,

$$\frac{dv_F}{dl} = \lambda^2(\mathcal{C}_1 - \mathcal{C}_2)v_F, \quad (\text{B9})$$

$$\frac{dv_\Delta}{dl} = \lambda^2(\mathcal{C}_1 - \mathcal{C}_3)v_\Delta, \quad (\text{B10})$$

$$\frac{d\frac{v_F}{v_\Delta}}{dl} = \lambda^2(\mathcal{C}_3 - \mathcal{C}_2)\frac{v_F}{v_\Delta}, \quad (\text{B11})$$

$$\frac{d\lambda}{dl} = \left[\mathcal{C}_1 - \mathcal{C}_2 + \frac{[(u_1)^2 + (u_2)^2 - (u_0)^2 - (u_3)^2]}{8\pi v_F v_\Delta} \right] \lambda^3, \quad (\text{B12})$$

$$\frac{du_0}{dl} = \left\{ -1 + 2\mathcal{C}_1 - \frac{(u_1 u_2 + u_2 u_3)}{4\pi v_F v_\Delta u_0} + \frac{2\lambda^2}{3} \left[\frac{u_2}{u_0}(\mathcal{C}_2 - \mathcal{C}_1) - 4\mathcal{C}_1 \right] \right\} u_0, \quad (\text{B13})$$

$$\frac{du_1}{dl} = \left\{ -1 + 2\mathcal{C}_1 + \frac{1}{4\pi v_F v_\Delta} (u_0 - u_1 - u_2 - 2u_3 + \frac{2u_2 u_3}{u_1}) + \frac{2\lambda^2}{3} \left[\frac{u_2}{u_1}(\mathcal{C}_3 - \mathcal{C}_2) - \mathcal{C}_1 - 5\mathcal{C}_3 \right] \right\} u_1, \quad (\text{B14})$$

$$\frac{du_2}{dl} = \left\{ -1 + 2\mathcal{C}_1 + \frac{1}{4\pi v_F v_\Delta} \left[(2u_0 - 3u_1 - 2u_2 - 3u_3) + \frac{2u_1 u_3}{u_2} \right] + \frac{2\lambda^2}{3} [4\mathcal{C}_2 - 5\mathcal{C}_1 - 5\mathcal{C}_3 + \frac{u_1}{u_2}(\mathcal{C}_3 - \mathcal{C}_2)] \right\} u_2, \quad (\text{B15})$$

$$\frac{du_3}{dl} = \left\{ -1 + 2\mathcal{C}_1 + \frac{1}{4\pi v_F v_\Delta} \left[(u_0 - u_3 - u_1 - 2u_2) + \frac{2u_1 u_2}{u_3} \right] + \frac{2\lambda^2}{3} \left[\frac{u_1}{u_3}(\mathcal{C}_2 - \mathcal{C}_1) - 4\mathcal{C}_2 \right] \right\} u_3, \quad (\text{B16})$$

for Type- τ_z , and

$$\frac{dv_\Delta}{dl} = \lambda^2(\mathcal{D}_1^{A,B} - \mathcal{D}_3^{A,B})v_\Delta, \quad (\text{B18})$$

$$\frac{dv_F}{dl} = \lambda^2(\mathcal{D}_1^{A,B} - \mathcal{D}_2^{A,B})v_F, \quad (\text{B17})$$

$$\frac{d\frac{v\Delta}{v_F}}{dl} = \lambda^2(\mathcal{D}_2^{A,B} - \mathcal{D}_3^{A,B})\frac{v\Delta}{v_F}, \quad (\text{B19})$$

$$\frac{d\lambda}{dl} = (\mathcal{D}_1^{A,B} - \mathcal{D}_1^{A,B})\lambda^3 = 0, \quad (\text{B20})$$

for Type- τ_0 phase transitions, respectively. It is worth pointing out that the Yukawa coupling λ is still marginal to the one-loop level and hence does not flow with the

decrease of energy scale. Given the fermion-fermion interactions can only indirectly influence the fermion velocities and accompanied physical implications via modifying such Yukawa coupling, we henceforth can safely skip the effects caused by fermion-fermion interactions, in other words neglecting the one-loop RG equations of the fermion-fermion interactions.

-
- [1] M. Sigrist and K. Ueda, *Rev. Mod. Phys.* **63**, 239 (1991).
- [2] E. Dagotto, *Rev. Mod. Phys.* **66**, 763 (1994).
- [3] V. J. Emery and S. A. Kivelson, *Nature*, **374**, 30 (1995).
- [4] M. Sigrist and T. M. Rice, *Rev. Mod. Phys.* **67**, 503 (1995).
- [5] M. Tinkham, *Introduction to Superconductivity, Dover Books on Physics Series*, Dover Publications, (1996).
- [6] P. W. Anderson, *The Theory of Superconductivity in the High-Tc Cuprate Superconductors*, Princeton University Press, (1997).
- [7] S. A. Kivelson, E. Fradkin, and V. J. Emery, *Nature (London)*, **393**, 550 (1998).
- [8] S. Sachdev, *Science* **288**, 475 (2000).
- [9] E. Dagotto, *Science* **309**, 257 (2005).
- [10] S. Sachdev and B. Keimer, *Phys. Today* **64**(2), 29 (2011).
- [11] M. Vojta, Y. Zhang, and S. Sachdev, *Phys. Rev. Lett.* **85**, 4090 (2000).
- [12] M. Vojta, Y. Zhang, and S. Sachdev, *Phys. Rev. B* **62**, 6721 (2000).
- [13] M. Vojta, Y. Zhang, and S. Sachdev, *Int. J. Mod. Phys. B* **14**, 3719 (2000).
- [14] S. Sachdev, *Rev. Mod. Phys.* **75**, 913 (2003).
- [15] S. A. Kivelson, I. P. Bindloss, E. Fradkin, V. Oganesyan, J. M. Tranquada, A. Kapitulnik, and C. Howald, *Rev. Mod. Phys.* **75**, 1201 (2003).
- [16] P. A. Lee, N. Nagaosa, and X. -G. Wen, *Rev. Mod. Phys.* **78**, 17 (2006).
- [17] Y. Huh and S. Sachdev, *Phys. Rev. B* **78**, 064512 (2008).
- [18] J. Wang, G. Z. Liu, and H. Kleinert, *Phys. Rev. B* **83**, 214503 (2011).
- [19] E. A. Kim, M. J. Lawler, P. Oreto, S. Sachdev, E. Fradkin, and S. A. Kivelson, *Phys. Rev. B* **77**, 184514 (2008).
- [20] C. Xu, Y. Qi, and S. Sachdev, *Phys. Rev. B* **78**, 134507 (2008).
- [21] J. H. She, J. Zaanen, A. R. Bishop, and A. V. Balatsky, *Phys. Rev. B* **82**, 165128 (2010).
- [22] J. H. She, M. J. Lawler, and E. A. Kim, *Phys. Rev. B* **92**, 035112 (2015).
- [23] E. Fradkin and S. A. Kivelson, *Nature Phys* **8**, 864 (2012).
- [24] H. Watanabe, A. Vishwanath, and S. A. Kivelson, *PNAS* **111**, 16314 (2014).
- [25] E. Fradkin, S. A. Kivelson, and J. M. Tranquada, *Rev. Mod. Phys.* **87**, 457 (2015).
- [26] P. W. Phillips, L. Yeo, and E. W. Huang, *Nat. Phys.* **16**, 1175 (2020).
- [27] A. Larkin and A. Varlamov, *Theory of fluctuations in superconductors*, Oxford University Press (New York), (2005).
- [28] H. Ding, T. Yokoya, J. C. Campuzano, T. Takahashi, M. Randeria, M. Norman, T. Mochiku, and J. Giapintzakis, *Nature (London)*, **382**, 51 (1996).
- [29] A. G. Loeser, Z. -X. Shen, D. S. Desau, D. S. Marshall, C. H. Park, P. Fournier, and A. Kapitulnik, *Science* **273**, 325 (1996).
- [30] T. Valla, A. Fedorov, P. Johnson, B. Wells, S. Hulbert, Q. Li, G. Gu, and N. Koshizuka, *Science* **285**, 2110 (1999).
- [31] J. Orenstein and A. J. Millis, *Science* **288**, 468 (2000).
- [32] T. Yoshida, X. J. Zhou, T. Sasagawa, W. L. Yang, P. V. Bogdanov, A. Lanzara, Z. Hussain, T. Mizokawa, A. Fujimori, H. Eisaki, Z. -X. Shen, T. Kakeshita, and S. Uchida, *Phys. Rev. Lett.* **91**, 027001 (2003).
- [33] M. Vojta, *Rep. Prog. Phys.* **66**, 2069 (2003).
- [34] P. Coleman and A. J. Schofield, *Nature*, **433**, 20 (2005).
- [35] S. Sachdev, *Quantum Phase Transitions*, 2nd edn., Cambridge University Press, Cambridge, (2011).
- [36] D. V. Khveshchenko and J. Paaske, *Phys. Rev. Lett.* **86**, 4672 (2001).
- [37] L. Fritz and S. Sachdev, *Phys. Rev. B* **80**, 144503 (2009).
- [38] G. -Z. Liu, J. -R. Wang, and J. Wang, *Phys. Rev. B* **85**, 174525 (2012).
- [39] J. -R. Wang and G. -Z. Liu, *New J. Phys.* **15**, 063007 (2013).
- [40] E. G. Moon and S. Sachdev, *Phys. Rev. B* **82**, 104516 (2010).
- [41] E. G. Moon and S. Sachdev, *Phys. Rev. B* **85**, 184511 (2012).
- [42] Y. Huh, E. -G. Moon, and Y. B. Kim, *Phys. Rev. B* **93**, 035138 (2016).
- [43] E. -G. Moon, *Sci. Rep.* **6**, 31051 (2016).
- [44] J. Wang, A. Eberlein, and W. Metzner, *Phys. Rev. B* **89**, 121116(R) (2014).
- [45] P. A. Lee, *Phys. Rev. Lett.* **71**, 1887 (1993).
- [46] C. Castellani, C. D. Castro, and M. Grilli, *Z. Phys. B: Condens. Matter* **103**, 137 (1997).
- [47] S. -X. Yang, H. Fotso, S. -Q. Su, D. Galanakis, E. Khatami, J. -H. She, J. Moreno, J. Zaanen, and M. Jarrell, *Phys. Rev. Lett.* **106**, 047004 (2011).
- [48] J. Wang, *Phys. Rev. B* **87**, 054511 (2013).
- [49] A. C. Durst and P. A. Lee, *Phys. Rev. B* **62**, 1270 (2000).
- [50] P. A. Lee and X. -G. Wen, *Phys. Rev. Lett.* **78**, 4111 (1997).
- [51] J. Mesot, M. R. Norman, H. Ding, M. Randeria, J. C. Campuzano, A. Paramakanti, H. M.

- Fretwell, A. Kaminski, T. Takeuchi, T. Yokoya, T. Sato, T. Takahashi, T. Mochiku, and K. Kadowaki, *Phys. Rev. Lett.* **83**, 840 (1999).
- [52] M. Vojta, *Adv. Phys.* **58**, 699 (2009).
- [53] C. J. Halboth and W. Metzner, *Phys. Rev. Lett.* **85**, 5162 (2000).
- [54] V. Oganesyan, S. A. Kivelson, and E. Fradkin, *Phys. Rev. B* **64**, 195109 (2001).
- [55] Y. Zhang, E. Demler, and S. Sachdev, *Phys. Rev. B* **66**, 094501 (2002).
- [56] H. Yamase and W. Metzner, *Phys. Rev. B* **75**, 155117 (2007).
- [57] V. Hinkov, D. Haug, B. Fauque, P. Bourges, Y. Sidis, A. Ivanov, C. Bernhard, C. T. Lin, and B. Keimer, *Science* **319**, 597 (2008).
- [58] S. Raghu, A. Paramekanti, E. -A. Kim, R. A. Borzi, S. A. Grigera, A. P. Mackenzie, and S. A. Kivelson, *Phys. Rev. B* **79**, 214402 (2009).
- [59] M. J. Lawler, K. Fujita, J. Lee, A. R. Schmidt, Y. Kohsaka, K. C. Kim, H. Eisaki, S. Uchida, J. C. Davis, J. P. Sethna, and E. -A. Kim, *Nature* **466**, 347 (2010).
- [60] E. G. Moon and S. Sachdev, *Phys. Rev. B* **82**, 104516 (2010).
- [61] E. -A. Kim and M. J. Lawler, *Phys. Rev. B* **81**, 132501 (2010).
- [62] E. Fradkin, S. A. Kivelson, M. J. Lawler, J. P. Eisenstein, and A. P. Mackenzie, *Annu. Rev. Condens. Matter Phys.* **1**, 153 (2010).
- [63] J. Wang and G. Z. Liu, *New J. Phys.* **15**, 073039 (2013).
- [64] J. Wang, *Phys. Lett. A* **379**, 1917 (2015).
- [65] B. Roy, *arXiv :2004.13043*, (2020).
- [66] S. Maiti and A. V. Chubukov, *Phys. Rev. B* **82**, 214515 (2010).
- [67] O. Vafek, *Phys. Rev. B* **82**, 205106 (2010).
- [68] V. Cvetković, R. E. Throckmorton, and O. Vafek, *Phys. Rev. B* **86**, 075467 (2012).
- [69] J. M. Murray and O. Vafek, *Phys. Rev. B* **89**, 201110 (2014).
- [70] R. Nandkishore, L. S. Levitov, and A. V. Chubukov, *Nature Phys.* **8**, 158 (2012).
- [71] R. Nandkishore, J. Maciejko, D. A. Huse, and S. L. Sondhi, *Phys. Rev. B* **87**, 174511 (2013).
- [72] A. V. Chubukov, M. Khodas, and R. M. Fernandes, *Phys. Rev. X* **6**, 041045 (2016).
- [73] S. Sur and R. Nandkishore, *New J. Phys.* **18**, 115006 (2016).
- [74] B. Roy, V. Juricic, and S. D. Sarma, *Sci Rep* **6**, 32446 (2016).
- [75] B. Roy, P. Goswami, and J. D. Sau, *Phys. Rev. B* **94**, 041101(R) (2016).
- [76] B. Roy and S. D. Sarma, *Phys. Rev. B* **94**, 115137 (2016).
- [77] R. M. Nandkishore and S. A. Parameswaran, *Phys. Rev. B* **95**, 205106 (2017).
- [78] B. Roy, *Phys. Rev. B* **96**, 041113 (2017).
- [79] B. Roy, Y. Alavirad, and J. D. Sau, *Phys. Rev. Lett.* **118**, 227002 (2017).
- [80] J. Wang, C. Ortix, J. van den Brink, and D. V. Efremov, *Phys. Rev. B* **96**, 201104(R) (2017).
- [81] J. Wang, *J. Phys. Condens. Matter* **30**, 125401 (2018).
- [82] Y. -M. Dong, D. -X. Zheng, and J. Wang, *J. Phys. Condens. Matter* **31**, 275601 (2019).
- [83] B. Roy, R. J. Slager, and V. Juričić, *Phys. Rev. X* **8**, 031076 (2018).
- [84] B. Roy and M. S. Foster, *Phys. Rev. X* **8**, 011049 (2018).
- [85] I. Mandal and R. M. Nandkishore, *Phys. Rev. B* **97**, 125121 (2018).
- [86] S. Sur and B. Roy, *Phys. Rev. Lett.* **123**, 207601 (2019).
- [87] J. Wang, *Nucl. Phys. B* **961**, 115230 (2020).
- [88] Y. H. Zhai and J. Wang, *Eur. Phys. J. B* **93**, 86 (2020).
- [89] Y. M. Dong, Y. H. Zhai, D. X. Zheng, and J. Wang, *Phys. Rev. B* **102**, 134204 (2020).
- [90] Y. H. Zhai and J. Wang, *Nucl. Phys. B* **966**, 115371 (2021).
- [91] A. L. Szabó and B. Roy, *Phys. Rev. B* **103**, 205135 (2021).
- [92] A. L. Szabó and B. Roy, *JHEP* **01**, 004 (2021).
- [93] S. E. Han, G. Y. Cho, and E. -G. Moon, *Phys. Rev. B* **95**, 094502 (2017).
- [94] B. Roy, V. Juričić, and I. F. Herbut, *JHEP* **04**, 018 (2016).
- [95] G. Y. Cho and E. -G. Moon, *Sci. Rep.* **6**, 19198 (2016).
- [96] S. -K. Jian and H. Yao, *Phys. Rev. B* **96**, 155112 (2017).
- [97] H. -K. Tang, J. N. Leaw, J. N. B. Rodrigues, I. F. Herbut, P. Sengupta, F. F. Assaad, and S. Adam, *Science* **361**, 570 (2018).
- [98] S. -X. Zhang, S. -K. Jian, and H. Yao, *Phys. Rev. B* **103**, 165129 (2021).
- [99] K. G. Wilson, *Rev. Mod. Phys.* **47**, 773 (1975).
- [100] J. Polchinski, *arXiv:hep-th/9210046* (unpublished).
- [101] R. Shankar, *Rev. Mod. Phys.* **66**, 129 (1994).
- [102] I. Makhfudz, *Annals of Physics* **360**, 113 (2015).
- [103] J. Wang and G. -Z. Liu, *Phys. Rev. B* **92**, 184510 (2015).
- [104] J. Wang, G. -Z. Liu, D. V. Efremov, and J. van den Brink, *Phys. Rev. B* **95**, 024511 (2017).
- [105] J. Wang, *arXiv: 2007.14981v1* (2020).
- [106] J. Orenstein, G. A. Thomas, A. J. Millis, S. L. Cooper, D. H. Rapkine, T. Timusk, L. F. Schneemeyer, and J. V. Waszczak, *Phys. Rev. B* **42**, 6342 (1990).
- [107] W. N. Hardy, D. A. Bonn, D. C. Morgan, R. Liang, and K. Zhang, *Phys. Rev. Lett.* **70**, 3999 (1993).
- [108] Y. J. Uemura, G. M. Luke, B. J. Sternlieb, J. H. Brewer, J. F. Carolan, W. N. Hardy, R. Kadono, J. R. Kempton, R. F. Kief, S. R. Kreitzman, P. Mulhern, T. M. Riseman, D. L. Williams, B. X. Yang, S. Uchida, H. Takagi, J. Gopalakrishnan, A. W. Sleight, M. A. Subramanian, C. L. Chien, M. Z. Cieplak, G. Xiao, V. Y. Lee, B. W. Statt, C. E. Stronach, W. J. Kossler, X. H. Yu, *Phys. Rev. Lett.* **62**, 2317 (1989).
- [109] M. Chiao, R. W. Hill, C. Lupien, L. Taillefer, P. Lambert, R. Gagnon, and P. Fournier, *Phys. Rev. B* **62**, 3554 (2000).